Supplementary Material for:

title: **Exploring the Correlation between the Cognitive Benefits of Drug Combinations in a Clinical Database and the Efficacies of the Same Drug Combinations Predicted from a Computational Model**

author: Thomas J. Anastasio

This supplement contains items that support the analysis presented in the above-referenced article, the purpose of which is to identify combinations of repurposed drugs that could be effective in the treatment of Alzheimer's disease (AD). The core idea is to overcome the limitations in available data by searching for correlations between representations of two completely different datasets: a database of clinical findings on dementia, and a computational model based on the pre-clinical literature on neuroinflammation. The dataset is provided by permission from the Rush Alzheimer's Disease Center (RADC database). The computational model was created on the basis of experimental data as published in the literature on microglia (MG model). This supplement contains figures and tables that support the narrative developed in the main text.

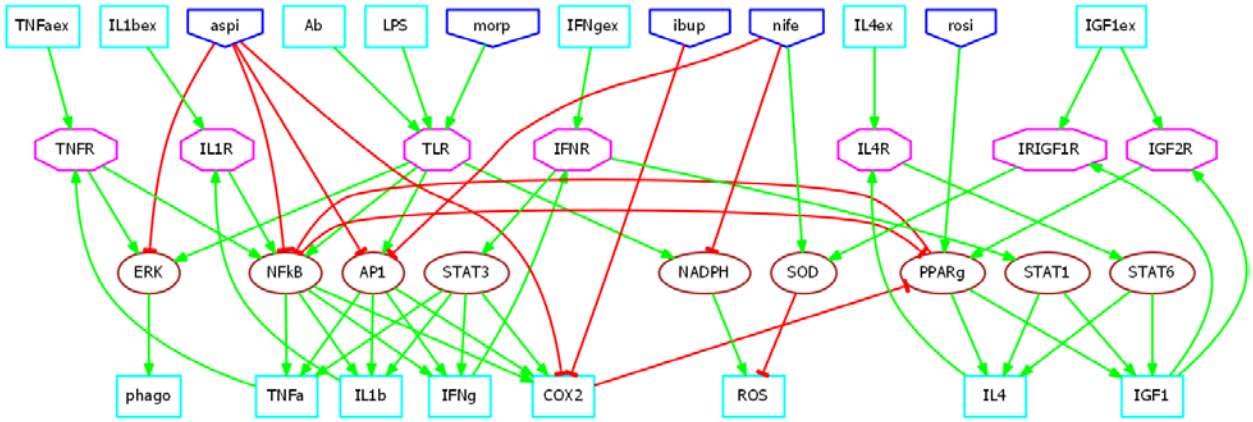

Fig. S1. Simplified schematic of the microglia (MG) model. The MG model recapitulates the structure of a microglial cell. Ligands (rectangles) bind receptors (octagons), which activate signaling molecules (ovals), which in turn activate transcription factors (also ovals), which modulate gene expression. Many of the microglial gene products (also rectangles) act as ligands for microglial receptors, forming many feedback loops. The presence/absence of certain factors distinguish young from old animals, or microglia extracted from them, such as acetylcholine and fractalkine (young) or necrotic factors (old). Drugs (trapezoids) can have one or more targets. Model elements are either inputs or units, which differ in that inputs cannot receive connections from other elements. This diagram is a highly simplified version of the full MG model, which is composed of 90 inputs and 146 units. See Tab. S1.

Tab. S1. Table of MG model elements and abbreviations. The name of each molecular species or cellular process is listed along with its abbreviation and the corresponding name of the element that represents it in the model. Each model element name is the same as the name used for it in the computer programs. Since the programming languages do not allow Greek characters they are replaced with lower-case Roman letters. To further distinguish model element names from actual molecule or cellular-process names they are rendered in monotype font. The # symbol in abbreviations or model element names stands for an arbitrary integer number. Abbreviations or model element names are not applicable (n/a) to items that are, respectively, not abbreviated in the text or do not appear in the current version of the model.

element name	**abbreviation**	**model element**
acetaminophen	n/a	`acet`
acetylcholine	Ach	`Ach`
acetylsalicylic acid (aspirin)	n/a	`aspi`
adaptor protein 1	AP1	`AP1`
adenosine monophosphate-activated protein kinase	AMPK	`AMPK`
adenylate cyclase	AC	`AC`
aldosterone	n/a	`aldo`
Alzheimer Disease	AD	`n/a`
amyloid-β	Aβ	`Ab`
amyloid-β internal	n/a	`AbIN`
anandamide	AEA	`AEA`
angiotensinogen	ang	`ang`
angiotensin I	angI	`angI`

angiotensin II	angII	angII
angiotensin II receptor #	AT#	AT#
angiotensin converting enzyme	ACE	ACE
apocynin	n/a	apoc
arachidonoylglycerol	2AG	AG
arginase 1	Arg1	Arg1
α # adrenergic receptor	a#AR	a#AR
α 6 β 1 integrin	α6β1	a6b1
α 7 nicotinic acetylcholine receptor	α7nAChR	a7nAChR
β-arrestin	bArr	bArr
β-2-adrenergic receptor	b2AR	b2AR
11-β-hydroxysteroid dehydrogenase	bHSD1	bHSD1
beclin-1	bec1	bec1
8-bromo-cyclic adenosine monophosphate	BrcAMP	BrcAMP
butenal	n/a	bute
c-Jun N terminal kinase	JNK	JNK
caffeine	n/a	caff
calcium	Ca	Ca
cannabinoid receptor #	CB#	CB#
caspase #	casp#	casp#
cathepsin B	n/a	cathB
Cay10512	Cay	Cay
chitinase-like protein	Ym1	Ym1
chloroquine	n/a	chlo
clonidine	n/a	clon
cluster of differentiation #	CD#	CD#
cluster of differentiation # ligand	CD#L	CD#L
cluster of differentiation # receptor	CD#R	CD#R
compound C	n/a	compC
cortisone	CORT	CORT
cyclic adenosine monophosphate	cAMP	cAMP
cyclic guanosine monophosphate	cGMP	cGMP
cytochrome C oxygenase #	COX#	COX#
cytoskeleton	n/a	cyto
dexamethasone	n/a	dexa
diacylglycerol lipase	DAGL	DAGL
dimethylfumarate	n/a	dime
diphenhydramine	diph	diph
diphenylene iodonium chloride	DPI	DPI
dithiocarbamate	PDTC	PDTC
docking protein #	Dok#	Dok#
DNA-X adaptor protein 12	DAP12	DAP12
edaravone	n/a	edar
E prosthanoid receptor #	EP#	EP#
E prosthanoid receptor 4-associated protein	EPRAP	EPRAP
estrogen (estradiol)	E2	E2

exchange protein activated by cAMP	Epac	Epac
extracellular signal-related kinase	ERK	ERK
Fas-associated protein with death domain	FADD	FADD
fibrillar Aβ	fAβ	n/a
flecainide	n/a	flec
fluoxetine	n/a	fluo
forkhead box protein O	FOXO	FOXO
fractalkine	CX3CL1	CX3CL1
fractalkine receptor	CX3CR1	CX3CR1
G protein-coupled estrogen receptor	GPER	GPER
G protein i	Gi	Gi
G protein q	Gq	Gq
G protein s	Gs	Gs
glimepiride	n/a	glim
glucocorticoid receptor	GR	GR
growth factor receptor binding protein 2	GRB2	GRB2
guanosine triphosphate-ase activating protein	GAP	GAP
guanylate cyclase	GC	GC
histamine	HA	HA
histamine 1 receptor	H1R	H1R
hydrogen sulfide	H2S	n/a
ibuprofen	n/a	ibup
inducible nitric oxide synthase	iNOS	iNOS
inhibitor of κ B	IκB	IkB
inhibitor of κ B kinase	IKK	IKK
inositol phosphate	IP	IP
insulin receptor	IR	n/a
insulin receptor insulin-like growth factor 1 receptor	IRIGF1R	IRIGF1R
insulin-like growth factor 1	IGF1	IGF1
insulin-like growth factor # receptor	IGF#R	IGF#R
interferon γ	IFNγ	IFNg
interferon receptor	IFNR	IFNR
interleukin #	IL#	IL#
interleukin 1 β	IL1β	IL1b
interleukin # receptor	IL#R	IL#R
interleukin 1 receptor-associated kinase	IRAK	IRAK
isoproterenol	isop	isop
Janus kinase #	JAK#	JAK#
JWH-015	n/a	JWH
lipopolysaccharide	LPS	LPS
lipoxin (or aspirin-triggered lipoxin)	n/a	lipo
lipoxin A4 receptor	ALX	ALX
lithium	Li	Li
liver tyrosine kinase	Lyn	Lyn
liver X receptor β	LXRβ	LXRb
liver X receptor β ligand	n/a	LXRbL

L-N-monomethyl arginine citrate	LNMMA	LNMMA
losartan	n/a	losa
LY294002	n/a	LY294
major histocompatibility complex 2	MHC2	n/a
MAPK/ERK kinase	MEK	MEK
mifepristone	n/a	mife
melatonin	n/a	mela
metformin	n/a	metf
mineralocorticoid receptor	MR	MR
minocycline	n/a	mino
mitogen-activated protein kinase	MAPK	MAPK
mitogen-activated protein # kinase	MAP#K	MAP#K
mitogen-activated protein kinase phosphatase #	MKP#	MKP#
morphine	n/a	morp
myeloid differentiation primary response protein	MyD88	MyD88
N-acetylcysteine	NAC	NAC
N-acyl phosphatidylethanolamine	NAPE	NAPE
naloxone	n/a	nalo
necrotic factors	n/a	necro
nicotine	n/a	nico
nicotinamide adenine dinucleotide phosphate (reduced)	NADPH	NADPH
nifedapine	n/a	nife
nitric oxide	NO	NO
N-(L-3-*trans*-Propylcarbonyl-oxirane-2-carbonyl)-L-isoleucyl-L-proline methyl ester	CA074Me	CA074
N-nitro-L-arginine methyl ester	LNAME	LNAME
non-steroidal anti-inflammatory drugs	NSAIDs	n/a
noradrenelin	NA	NA
nuclear factor κ B	NFκB	NFkB
nucleotide-binding-domain leucine-rich-repeat family pyrin domain containing 3 (cryopyrin 3)	NLRP3	NLRP3
omeprazole	n/a	omep
PD123319	n/a	PD123
pentoxifylline	n/a	pent
perindopril	n/a	peri
peroxisome proliferator-activated receptor γ	PPARγ	PPARg
PF-04418948	n/a	pf04
phagocytosis	n/a	phago
phenylephrine	n/a	phen
phosphatidylinositol 3 kinase	PI3K	PI3K
phosphodiesterase	PDE	PDE
phosphodiesterase 5	PDE5	PDE5
phosphoinositide 3 kinase	PI3K	PI3K
phospholipase A 2	PLA2	PLA2
phospholipase C	PLC	PLC
propentofylline	n/a	prope

propranolol	n/a	prop
prostaglandin E 2	PGE2	PGE2
protein kinase A	PKA	PKA
protein kinase B	Akt	Akt
protein kinase C	PKC	PKC
protein kinase Cδ	PKCδ	PKCd
protein kinase G	PKG	PKG
protein phosphatase 2 A	PP2A	PP2A
protein 38 mitogen-activated protein kinase	p38MAPK	p38MAPK
punicalagin	n/a	puni
Rac member of the Rho family of GTPases	Rac	Rac
Ras member of the Rho family of GTPases	Ras	Ras
rapidly accelerated fibrosarcoma 1	Raf1	Raf1
reactive oxygen species	ROS	ROS
receptor-interacting protein 1	RIP1	RIP1
renin	n/a	renin
repressor/activator protein 1	Rap1	Rap1
resveratrol	n/a	resv
retinoic acid	n/a	retino
retinoid X receptor	RXR	RXR
rifampicin	n/a	rifa
rosiglitazone	n/a	rosi
sarcoma homology domain 2-containing inositol phosphatase 1	SHIP1	SHIP1
SB203580	SB203	SB203
scavenger receptor A	SRA	n/a
scutellarin	n/a	scut
signal transducer and activator of transcription #	STAT#	STAT#
sildenafil	n/a	sild
Sma and Mad proteins from *C. elegans* and *Drosophila*, respectively	Smad	Smad
sodium	Na	Na
sodium hydrosulfide	NaHS	NaHS
sodium nitroprusside	SNP	SNP
spleen tyrosine kinase	Syk	Syk
spironolactone	n/a	spir
SP600126	SP600	SP600
superoxide dismutase	SOD	SOD
suppressor of cytokine signaling 3	SOCS3	SOCS3
tetrodotoxin	TTX	TTX
thalidomide	n/a	thal
Toll-like receptor #	TLR#	TLR#
Toll/interleukin 1 receptor (TIR)-domain-containing adaptor-inducing interferon β	TRIF	TRIF
TNF receptor-associated factor 6	TRAF6	TRAF6
transforming growth factor β	TGFβ	TGFb

transforming growth factor-associated kinase 1	TAK1	TAK1
transforming growth factor receptor	TGFR	TGFR
triggering receptor expressed on myeloid cells 2	TREM2	TREM2
triggering receptor expressed on myeloid cells 2 ligand	TREM2L	TREM2L
tumor necrosis factor α	TNFα	TNFa
tumor necrosis factor receptor	TNFR	TNFR
tumor necrosis factor receptor type 1-associated death domain protein	TRADD	TRADD
Vav guanine nucleotide exchange factor	Vav	Vav
voltage gated calcium channel	VGCC	VGCC
voltage gated sodium channel	VGSC	VGSC
WIN55,212-2 (cannabinoid receptor agonist)	WIN	WIN
wortmannin	n/a	wort

Tab. S2. List of MG model drugs, abbreviations, effects, targets, and references. The name of each drug is listed along with its model element name, in monotype. Also indicated in brackets are drugs in common between the MG model and the RADC database, which are included in the computational drug screen.

drug	effect(s)	target(s)	references
acetaminophen (acet) [in screen]	reduces LPS-induced COX2	COX2	[1]
acetylsalicylic acid (aspirin, aspi) [in screen]	reduces LPS-induced IL1b	COX2, ERK, IkB, and p38MAPK	[2, 3]
apocynin (apoc)	reduces HA-induced phago and ROS	NADPH	[4]
8-bromo-cyclic adenosine monophosphate (BrcAMP)	blocks LPS-induced increase in IL6, NO, and TNFa	cAMP	[5]
butenal (bute; and a more stable derivative)	reduces LPS-induced COX2, iNOS, NO, ROS, and TNFα	IκB, STAT1, and STAT3	[6, 7]
caffeine (caff)	reduces LPS- induced COX2, iNOS, NO, and TNFα	PDE	[8]
Cay10512	reduces aldosterone-induced increase in IL6	NFκB	[9]
CA-074 (CA074)	reduces Aβ-induced IL1β	cathB	[10]
chloroquine (chlo) [in screen]	reduces LPS-induced IL6, IL12, TNFα, and IL10	PLA2	[11]
clonidine (clon) [in screen]	does not reduce LPS-induced IL1b, IL6, iNOS,NO, and TNFa	α2AR	[5, 12]
compound C (compC)	prevents metf or resv suppression of morp-induced increases in IL1b, IL6, iNOS, and TNFa	AMPK	[13, 14]

dexamethasone (dexa) [in screen]	reduces LPS-induced IL6 and TNFα	MKP1	[15]
dimethylfumarate (dime)	reduces LPS- induced iNOS, NO, IL1β, IL6, and TNFα	ERK	[16]
diphenhydramine (diph) [in screen]	reduces HA-induced IL6, phago, ROS, and TNFa	H1R	[4, 17, 18]
diphenylene iodonium chloride (DPI)	reduces LPS/IFNg-induced iNOS, NO, IL1β, IL6, ROS, and TNFα	NADPH	[19-21]
dithiocarbamate (PDTC)	reduces HA-induced IL6 and TNFα	NFκB	[17]
edaravone (edar)	reduces LPS-induced NO, IL1β, ROS, and TNFα; reduces necroL-induced iNOS, IL1β, and TNFα	AT1, ROS	[22]
estrogen (estradiol; E2) [in screen]	reduces LPS-induced IL1β and TNFα	GPER	[23]
flecainide (flec; results on safinamide included) [in screen]	reduces LPS-induced ROS and necroL-induced iNOS	VGSC	[24]
fluoxetine (fluo) [in screen]	reduces LPS- induced iNOS, NO, IL6, and TNFα; enhances IL4-induced IL10	p38MAPK and IκB	[25, 26]
glimepiride (glim) [in screen] [averaged with rosi]	reduces LPS-induced IL1β, IL6, and TNFα	IGF2R and IRIGF1R	[27]
ibuprofen (ibup) [in screen]	reduces Aβ-induced COX2, IL1β, and ROS but enhances phago	COX2	[28-30]
isoproterenol (isop)	reduces LPS-induced iNOS and TNFα; enhances LPS-induced IL10; reduces LPS/IFNγ-induced IL12	β2AR	[31-33]
JWH-133 or JWH-015 (JWH)	induces IL10; reduces LPS-induced TNFα; rescues CD40L-impaired phagocytosis of Aβ; reduces IFNγ/CD40L-induced NO and TNFα; reduces Aβ/CD40L-induced NO and TNFα;	CB2	[34, 35]
lipoxin (or aspirin-triggered lipoxin; lipo)	reduces LPS-induced iNOS, NO, IL1β, and TNFα	ALX	[36]
lithium (Li) [in screen]	Reduces LPS-induced IL1b, IL6, and TNFα	PI3K	[37, 38]
L-NMMA (LNMMA)	reduces LPS-induced NO and TNFα	iNOS	[39]

losartan (losa; candesartan results included) [in screen]	reduces LPS-induced COX2, IL1b, iNOS, NO, ROS, and TNFa but increases IL10	AT1R	[40-43]
melatonin (mela)	reduces LPS-induced iNOS, NO, IL1β, TNFα, and phagocytosis; reduces Aβ-induced IL6, ROS, and TNFα	NFκB	[44-46]
metformin (metf)	reduces morp-induced increases in IL1b, IL6, and TNFa	AMPK	[14]
mifepristone (mife)	increases IL6; reverses CORT- or dexamethazone-induced decrease in IL6; does not affect aldosterone-induced increase in IL6	MR	[9]
minocycline (mino) [in screen] [averaged with rifa]	reduces LPS-induced IFNγ, IL1β, iNOS, NO, and TNFα; does not affect IL4-induced IL4, IL10, or Arg1	NFκB	[20, 47, 48]
morphine (morp) [in screen]	increases IL1b, IL6, iNOS, NO, and TNFa but does not change IL4, IL10, or TGFb	MyD88	[13, 14, 49, 50]
N-acetylcysteine (NAC)	reduces Aβ-induced IL1β; reduces LPS-induced iNOS, NO, and ROS	ROS	[10, 19-21]
N-nitro-L-arginine methyl ester (LNAME)	reduces LPS-induced ROS	iNOS	[21]
naloxone (nalo)	reduces LPS-induced IL1β and TLRα	TLR4	[51, 52]
nicotine (nico)	reduces LPS-induced ROS and TNFα; reduces Aβ-induced ROS and TNFα; enhances phago generally	α7nAChR	[53-55]
nifidipine (nife; results on verapamil also included) [in screen]	reduces LPS-induced NO, ROS, and TNFα; reduces LPS/IFNg-induced COX2, IL1b, IL6, iNOS, NO, and TNFa; does not reduce LPS/IFNγ-induced phago	VGCC, NADPH, Akt, and p38MAPK	[56-58]
omeprazole (omep; results on lansoprazole also included) [in screen]	reduces LPS/IFNγ-induced TNFα	p38MAPK	[59]
PD123319 (PD123)	blocks decrease in LPS-induced COX2, IL1b, iNOS, NO, ROS, and TNFa and increase in IL10 due to losartan	AT2R	[42]
pentoxifylline (pent)	reduces LPS-induced IL1β and TNFα but not IL6 or NO	PDE	[15, 39]
perindopril (peri; results on captopril also included) [in screen]	reduces LPS-induced NO, ROS, and TNFα but increases IL10	ACE	[42, 60]

PF-04418948 (PF04; results on TG4-155 also included) [in screen]	reduces PGE2-induced COX2; reduces LPS/IFNγ/PGE2-induced IL6 but enhances TNFα	EP2	[61-63]
phenylephrine (phen)	reduces LPS-induced	α1AR	[5, 12, 64]
propranolol (prop) [in screen]	prevents isop from reducing LPS-induced iNOS, NO, and ROS	β2AR	[64, 65]
punicalagin (puni)	reduces LPS-induced COX2, IL6, and TNFα; reduces Aβ-induced TNFα	IKK	[66, 67]
resveratrol (resv)	reduces LPS-induced COX2, iNOS, NO, IL6, and TNFα; reduces LPS/IFNg-induced NO, IL1β, IL6, IL12, and TNFα; reduces Aβ-induced IL6 and TNFα; reduces morphine-induced increases in IL1b, IL6, iNOS, and TNFa; does not affect IL4, IL10, or TGFb	TLR4	[13, 68-70]
rifampicin (rifa) [in screen] [averaged with mino]	reduces LPS-induced COX2, iNOS, NO, IL1β, and TNFα	TLR4	[71, 72]
rosiglitazone (rosi; and also pioglitazone) [in screen] [averaged with glim]	reduces LPS-induced iNOS and IL1β; reduces Aβ-induced COX2 and iNOS but enhances phago; reduces necroL-induced NO and IL1β	PPARγ	[73-75]
SB203580 (SB203)	reduces HA-induced IL6 and TNFα	p38MAPK	[17]
scutellarin (scut)	reduces LPS-induced iNPS, NO, IL1β, ROS, and TNFα; reduces IFNγ-induced iNOS and NO; reduces necroL-induced iNOS, IL1β, and TNFα	JNK, p38MAPK, and STAT1	[22, 76]
sildenafil (sild)	reduces LPS-induced iNOS, NO, IL1β, ROS, and TNFα; reduces necroL-induced IL1β and TNFα but increases iNOS, NO, and IL10	PDE5	[20, 77]
sodium hydrosulfide (NaHS)	reduces Aβ-induced COX2, IL1β, IL6, and TNFα	NFκB	[78]
spironolactone (spir) [in screen]	reduces aldosterone-induced increase in IL6	MR	[9]
SP600126 (SP600)	reduces HA-induced IL6 and TNFα	JNK	[17]
tetrodotoxin (TTX)	reduces LPS-induced phagocytosis	VGSC	[79]
thalidomide (thal)	reduces LPS-induced IL6, NO, and TNFα	MyD88	[39, 80]
WIN-552122 (WIN) [in screen]	reduces LPS-induced iNOS and NO but has no effect on TNFα; reduces Ab-induced TNFα	CB1, CB2	[81, 82]
wortmannin (wort)	reduces HA-induced IL6 and TNFα	PI3K	[17]

Text S1. Optimizing the parameters of the MG model

The elements in the recurrent network model of microglia (MG model) can be divided into inputs and units. Units receive connections from the input elements and from the other units in the network. Input elements do not receive connections from other elements. The parameters of the MG model are the strengths (or weights) of the connections between model elements and they are optimized by training the model using a recurrent neural network learning algorithm [83, 84].

The algorithm is used to train the MG model on input/desired-output patterns that are hand curated from the result of experiments on microglia as reported in the literature. Tab. S3 shows a highly simplified version of the input/desired-output patterns, arranged in tabular form, that were used to train the MG model. The table shows that inputs are represented as binary (0 or 1), while desired outputs are assigned integer values in the range from 3 (low level) to 7 (high level), with a baseline of 5. The input/desired-output patterns used to train the model are discretized in order to regularize the highly non-standardized data available on microglia and the semi-quantitative techniques (such as gel electrophoresis, immunoprecipitation, etc) used to gather them. In the relatively few cases where different labs measured the effects on microglia of the same input pattern, the results of the different labs were combined to form a single input/desired-output pattern. This prevented overtraining the model on specific inputs that, through experimental bias, are better represented than others in the literature. Consistency between the findings of various labs was generally high. In the very few cases of disagreement between labs, the consensus was found and was represented in the input/desired-output table. The desired-output integer levels are scaled by 0.1 to being them into the [0, 1] range of the sigmoidal function that is used to model the activations of all model units.

On each training cycle an input/desired-output pattern is chosen at random from the input/desired-output table and the actual response of the network is computed. Because the model is a dynamical system its response is a function of time, and its actual output is taken after the network has reached steady state. Then network error is computed as the difference between the desired output and the actual output, and this error is used by the recurrent neural network learning algorithm to compute changes to the connection weights that reduce the error. The weight changes (either positive or negative) are scaled by a learning rate and are then added to the corresponding connection weights.

The number of training cycles greatly exceeds the number of input/desired-output training patterns, so each pattern is randomly chosen and applied many times to the network over the course of training. In the recurrent network model any input element or unit can connect with any other unit, so its connectivity is “complete” but all connections are not treated equally. Known structure is imposed on the network through differential learning weights. Many of the known cell-signaling interactions of microglia are recapitulated in the model by designating the connections between specific elements (eg from the transcription factor NFkB to the enzyme COX2, see also Fig. S1) as “structure” connections; the rest are designated as “non-structure connections”. To privilege the known structure connections over the non-structure connections the learning rate is three orders of magnitude higher for the structure than for the non-structure connection weights.

The model is trained over many training cycles (1×10^6), after which the mean squared error over all of the outputs and over all of the patterns is reduced to a very low value ($\sim 3 \times 10^{-4}$). Fig. S2 shows that the responses of the output units to all of the input patterns reaches steady state in under 25 time steps, and that the steady-state output responses closely match the desired outputs for all input/desired-output patterns (the mean squared error between the desired and actual outputs is less than 3×10^{-4}).

Tab. S3. Simplified MG model input/desired-output table. The microglia (MG) model is trained on pairs of input/desired-output patterns. Inputs (drugs or exogenous) are present or absent (1 or 0), while endpoint (target) outputs are assigned integer values between 3 (lowest) to 7 (highest). The actual input/desired-output training set contains 179 pairs of input/desired-output patterns.

input										**desired output**				
aspi	**ibup**	**morp**	**nife**	**rosi**	**Aβ**	**LPS**	**IL4ex**	**IGF1ex**		**IL1β**	**TNFα**	**ROS**	**IL4**	**IGF1**
0	0	0	0	0	0	0	0	0		**5**	**5**	**5**	**5**	**5**
0	0	0	0	0	**1**	0	0	0		**7**	**7**	**7**		**3**
0	0	0	0	0	0	**1**	0	0		**7**	**7**	**7**	**5**	**3**
0	0	0	0	0	0	0	**1**	0		**4**	**4**		**7**	**7**
0	0	0	0	0	0	0	0	**1**			**3**	**3**		
1	0	0	0	0	0	**1**	0	0		**6**	**6**			
0	**1**	0	0	0	**1**	0	0	0		**6**		**6**		
0	0	**1**	0	0	0	0	0	0		**7**	**7**		**5**	
0	0	0	**1**	0	0	**1**	0	0			**6**	**5**		
0	0	0	0	**1**	**1**	0	0	0		**6**	**6**		**7**	

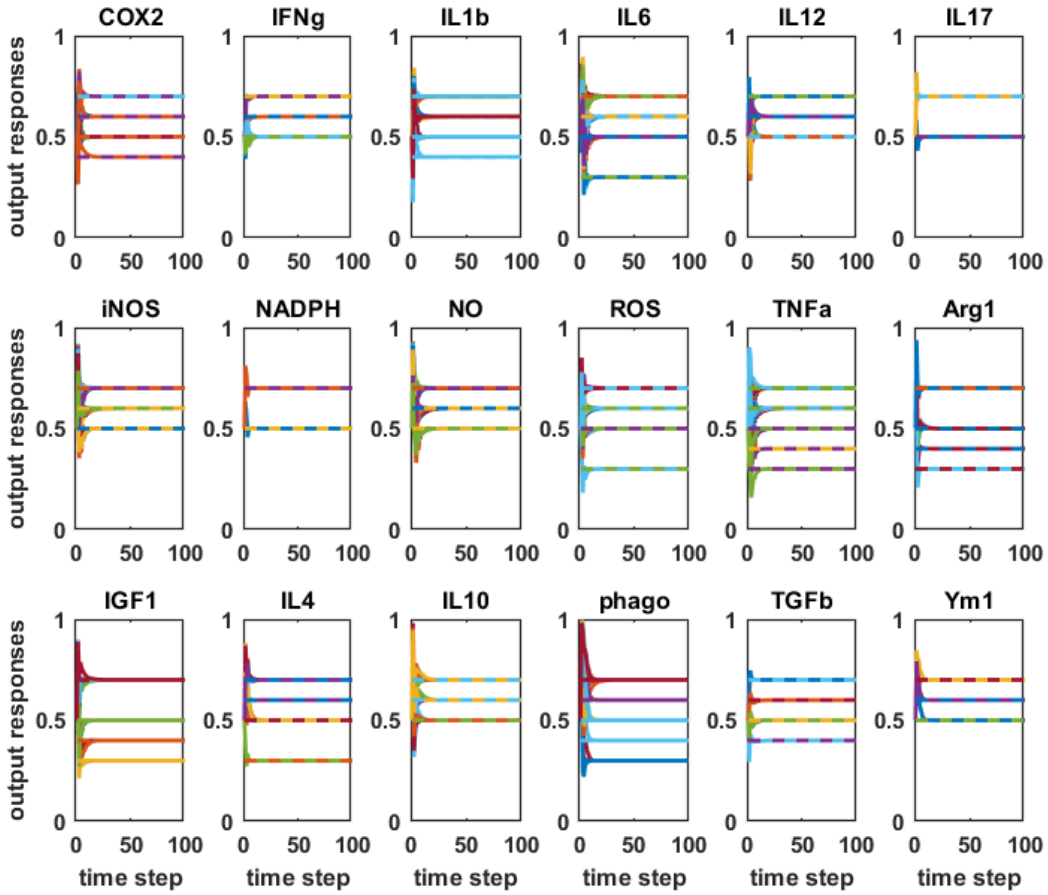

Fig. S2. Desired and actual outputs of an example trained MG model network. The trained MG model accurately reproduces the required input-output behavior. Eighteen model units are designed as target (endpoint) outputs because they represent factors (or in one case a process, phagocytosis) whose expression has been experimentally measured. Each subplot corresponds to 1 of the 18 output units and shows the agreement between its response (solid line) and each of the desired outputs (dashed lines) that it is assigned in the input/desired-output table. All of the actual output responses reach steady-state levels within 25 time steps, and the error between the desired and actual outputs is computed from the steady-state responses. The mean squared error between all of the actual and desired outputs less than 3×10^{-4}.

Text S2. The MG model and its identity as a deep neural network

The MG model aims to maximally utilize available experimental data on microglia by adhering to the known structure of microglial cell-signaling and gene regulatory pathways, and by conforming to the known behavior of microglia. Because of its autocrine (and paracrine) loops and its many other loops the model is a recurrent and therefore dynamic system, and it is modeled as a dynamic, recurrent network. Each element (input or unit) can influence the activation of other network units according to its own activation, and to the strength (or weight) of its connection to the units. Each unit computes the weighted sum of its activated connections from other elements and passes that sum through a sigmoidal (S-shaped) nonlinearity that bounds the activation of the unit between 0 and 1. The sigmoid represents the natural constraints on biological entities such as enzymes and other proteins whose expressions, concentrations, and activations are bounded from below at zero and from above at some saturation level. Recurrent networks of nonlinear elements, and particularly of sigmoidal elements, are commonly used in neurobiology to model systems of interacting neurons [85] but they can also serve as valid models of biological systems more generally [86].

The modeling approach taken here is analogous to many recent deep-learning approaches in two important respects. The first concerns the nature of “deep” networks. The term “deep learning” applies to feedforward neural networks of nonlinear elements where the first layer is the input layer, the last layer is the output layer, and all intervening layers are referred to as “hidden” layers. Activation in feedforward networks is propagated forward only, from the input layer through each successive hidden layer and finally to the output layer. The feedforward networks used in deep learning are “deep” because they have many hidden layers, and this greatly increases their processing power.

Recurrent neural networks can have specific input elements, and can also have specific units designated as outputs, but otherwise any unit can project to any other unit so recurrent networks have many interacting feedback loops but they lack explicit layers. However, recurrent neural networks are dynamic systems and, as such, their unit activations are functions of time. On each time step, each unit receives the weighted activations of other network elements on the previous time step, so that each time step in a recurrent network is equivalent to a hidden layer in a purely feedforward network [87]. A trained recurrent network that reaches steady-state in 25 time steps is equivalent to a feedforward network that is 25 layers deep.

The second respect in which this approach is analogous to many deep-learning approaches is in its incorporation of preset structure. Generally in feedforward networks the connectivity from a previous to a subsequent layer is “complete” in that every element in one layer connects to every element in the next layer. Convolutional neural networks are distinguished from other feedforward networks in having some layers whose connections to the next layer are not complete but are constrained according to the center-surround receptive field pattern that has been well described in the visual system [88, 89]. These layers are “convolutional” because the same connectivity pattern is applied in an overlapping fashion over the entire layer, but the key concept is that the known structure of a biological system can be incorporated into the structure of a neural network model to improve its performance. Thus, the center-surround receptive field structure that is preset in convolutional neural networks follows from the known physiology of the visual system, and it greatly improves the ability of convolutional neural networks to process images.

By analogy, many aspects of the known structure of the cell-signaling system of microglia has been incorporated into the recurrent neural network model, in an attempt to improve its ability to simulate the behavior of actual microglia (Fig. S1). The main structural feature of microglia recapitulated by the model is recurrence, which models known autocrine/paracrine interactions. Further structure is imposed on the recurrent network by allowing the weights of structure connections, which correspond to known interactions between elements of the model, to grow more rapidly than those of the non-structure weights during the training process (Text S1).

Where this approach most strikingly departs from the usual deep-learning approach is in the number of training examples available to train it. Most deep networks are trained on "big data", characterized by thousands of training examples. For example, a convolutional network was recently used to predict the disease status of patients from MRI images of their brains [90]. The network was trained on 2265 images of the brains of 755 patients from the Alzheimer Disease Neuroimaging Initiative (ADNI) who had been diagnosed and classified by neurologists as Alzheimer Disease (AD), mild cognitive impairment (MCI), or healthy control (HC). As images, all of the training inputs are from the same "domain", and so the trained network is expected to generalize well and to predict disease status (AD, MCI, or HC) given brain-scan images that were not included in the training set. Also, with over two thousand image/disease pairs in the ADNI database, there were sufficiently many for them to be divided into a training set and a testing set. Networks were trained only over the training set and then tested for generalizability using the testing set, and the experimenters used generalizability to choose between convolutional networks having two different structures.

The "small data" on which the recurrent network model of microglia was trained precludes this kind of testing/training regime for two reasons. First, with only 179 training pairs, the available training set is already very small. For example, it is more than an order of magnitude smaller than the ADNI image/disease set. Second, most of the inputs are from different domains, especially drug inputs. Ideally, the model should be trained on the results of many different experiments measuring the effects of the same drug or drug combination on the expressions of the same, large set of cytokines and other factors. Unfortunately, for many of the drugs included in this analysis, only one experiment was available that measured its effects on microglia, and then only measured its effects on one or a few cytokines and other factors (these drugs included acetaminophen, chloroquine, flecainide, glimepiride, omeprazole, and spironolactone; see Tab. S2 for other such compounds).

The trained model was needed to predict the effects of drugs in combination, but very few experiments measuring the effects on microglia of drugs in combination have been reported in the literature. Thus, experimental data is not available in a quantity sufficient both to train a model of microglia on drug combinations and to test its generalizability over drug combinations. To overcome these limitations, the approach taken here leveraged existing data both by structuring the model using information on known interactions within microglia, and then by training it using as much information as was available on the outputs of microglia to various drugs and other inputs. The fact that the efficacies of drug combinations in reducing neuroinflammation as predicted by the MG model are significantly correlated with the benefits of those same drug combinations as observed in the RADC database strongly suggests that the approach taken here was indeed effective in creating a model that captured important aspects of the behavior of actual brain microglia. The model's ability to predict drug-combination efficacy from an entirely new domain is proof of its generalization capability that is far more compelling than its performance on a testing set taken from the same dataset as its training set.

Text S3. Quantifying drug combination efficacy as predicted from the MG model

The predicted efficacy of any drug or drug combination can be defined by the amount by which it moves the response of the microglia model from the neurotoxic (highly pro-inflammatory) to the neuroprotective (highly anti-inflammatory) output pattern. The neurotoxic and neuroprotective output patterns, as well as the actual output pattern resulting from any drug or drug combination given in conjunction with Aβ and LPS, can be expressed as vectors each having 18 elements. Efficacy is then computed as the normalized difference between the actual (**a**) and neurotoxic (**t**) pattern vectors, divided by the sum of the normalized differences between the actual and neurotoxic, and the actual and neuroprotective (**p**) pattern vectors. Symbolically: efficacy = $|\mathbf{a}-\mathbf{t}| / (|\mathbf{a}-\mathbf{t}| + |\mathbf{a}-\mathbf{p}|)$, where $|*|$ denotes vector normalization. Thus, the vector norms are combined in a ratio that takes value 0 if the actual output pattern is the same as the neurotoxic pattern, value 1 if the actual output pattern is the same as the neuroprotective pattern, ½ if the actual output pattern is equally distant from the neurotoxic and neuroprotective patterns, et cetera. As explained in the main text, the analysis is focused on a specific set of 196 drug combinations. For illustrative purposes, the MG model efficacies of these 196 drug combinations are converted to angles and are shown in a polar plot in Fig. S3. The figure shows that the efficacies of different drug combinations as predicted by the MG model can vary considerably.

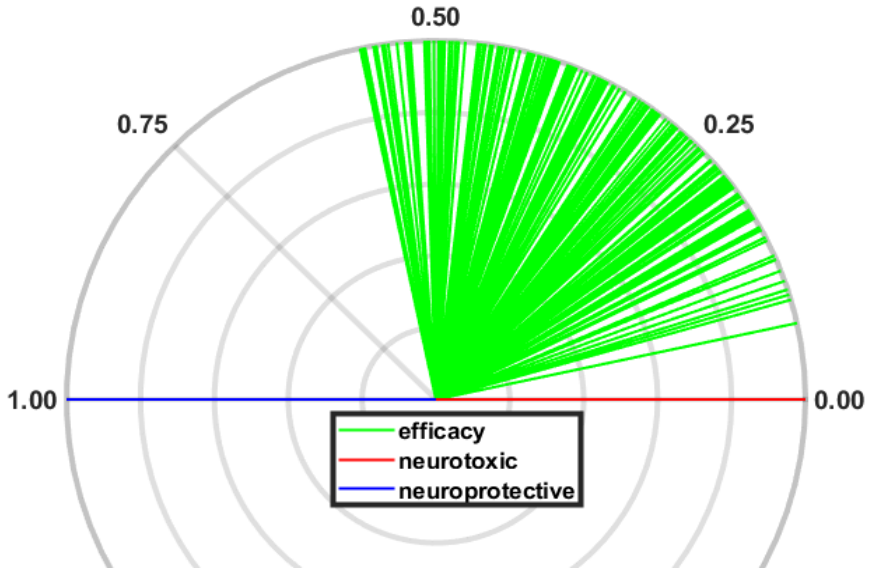

Fig. S3. Predicting the efficacy of drug combinations using the MG model. The MG model efficacy of any drug combination is quantified as the amount by which it can move the actual MG model output pattern from the neurotoxic (highly pro-inflammatory) to the neuroprotective (highly anti-inflammatory) pattern. The neurotoxic and neuroprotective output patterns are represented as vectors that are 180 degrees apart in 2-D space. Then each drug combination efficacy is converted to an angle, where efficacies from 0 to 1 correspond to angles from 0 to 180, and is represented as a vector in the same 2-D space. The "speedometer" (polar) plot shows the MG model efficacies of each of the 196 drug combinations that were included in the analysis. The speedometer representation is adopted for ease of illustration only. MG model efficacy is basically computed as a ratio of differences between patterns, which are expressed in terms vectors and norms for ease of computation (see Text S3). No assumption of the orthonormality of an 18-dimensional vector space containing the output patterns is intended.

Text T4. Assessing drug combination benefit from the RADC database

Assigning a numerical value to RADC benefit required a number of steps, but the number of simplifying assumptions was kept to a minimum. The first step was to rescale the raw scores on the 25 different assessments of cognitive function, since each was quantified according to its own scale. For example, in the "animals" test, participants named as many different animals as they could over several 1 minute trials, and the number of animals named ranged from 0 to 75. The raw scores on this test where therefore rescaled into the range [0, 1] by dividing each score by 75. The scores on the other 24 tests were similarly rescaled, and then the various rescaled scores for each participant were averaged to form a composite cognitive score for each visit.

A key challenge in the analysis of the RADC dataset is the well-known relationship between cognitive function and age, so the age variable must be taken into account in assessing the relative benefits of the various drug combinations. Adding to the challenge is the fact that cognitive function was assessed at different ages for different participants. To meet this challenge, the decline of cognitive function with age for all of the participants in each drug combination group was summarized by pooling all of the composite cognitive score versus age (cog-score vs age) values for all participants in each drug combination group, and fitting them with a simple power function via nonlinear regression. The power function relates cog-score to age by raising age to an exponent (*n*), multiplying that power by a scalar (*s*), and summing that product with a constant (*c*). Symbolically: expected cog-score = *s* * age ^ *n* + *c*. Fitting of the power function to cog-score vs age data is illustrated in Fig. S4A for a specific drug category case and for the no-drug case. Note that the expected cog-score at any age is the cog-score as computed by the best-fit power function, after the observed cog-score vs age data are used to parameterize the power function.

The power functions fit to cog-score vs age data for all 196 of the main drug combinations, along with the power function fit to the no-drug cog-score vs age data, are shown in Fig. S4B. The curves in Fig. S4B show that cog-score vs age relationships vary considerably between different drug combination groups, and that cognitive function in many drug combination groups is worse than that in the no-drug group.

Finally, to reduce the RADC database benefit of any specific drug combination to a single value, the power function curve for that group was used to compute the expected cog-score at each age included in that specific drug combination group (pooled over all participants in that group). Also, the power function curve for the no-drug group was used to the compute the expected cog-score in the no-drug case, but at the same ages as were included for that specific drug combination group. Then, the expected cog-score in the no-drug case was subtracted from the expected cog-score for that specific drug combination *at the same set of ages*, and the differences were average to yield the RADC database benefit for that specific drug group.

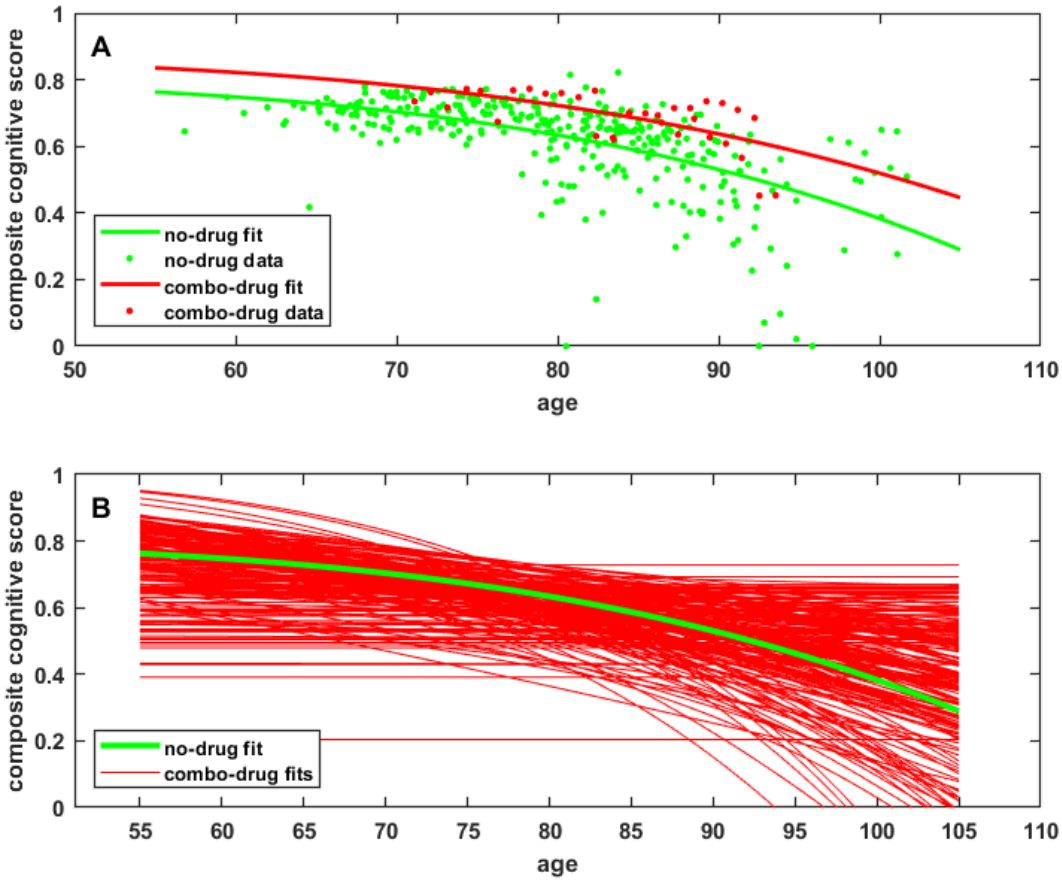

Fig. S4. Fitting power functions to composite cognitive score versus age data. The RADC database benefit of any drug combination is quantified as the average difference between the composite cognitive scores of RADC participants who took that drug combination (drug-combo group) and those who took no drugs (no-drug group). Cognitive score as a function of age is described using a power function whose parameters are optimized to provide the best fit to the data in a least-squares sense. Panel (A) shows the power functions fit to the age vs composite cognitive scores for the RADC participants who took no drugs, and for those who took a specific, representative drug combination. The fitted power functions are then used to compute the expected composite cognitive scores for the drug and no-drug groups at the ages for which the drug group data are available, and the average of the differences (drug – no-drug) is computed. Panel (B) shows the power functions best fit to the data of the no-drug group (81 participants) and to the groups of RADC participants who each took 1 of the 196 drug combinations included in the analysis (1045 participants total over all 196 drug groups). This plot shows that most of the RADC database benefits are negative, so RADC database benefit should be interpreted as a relative measure.

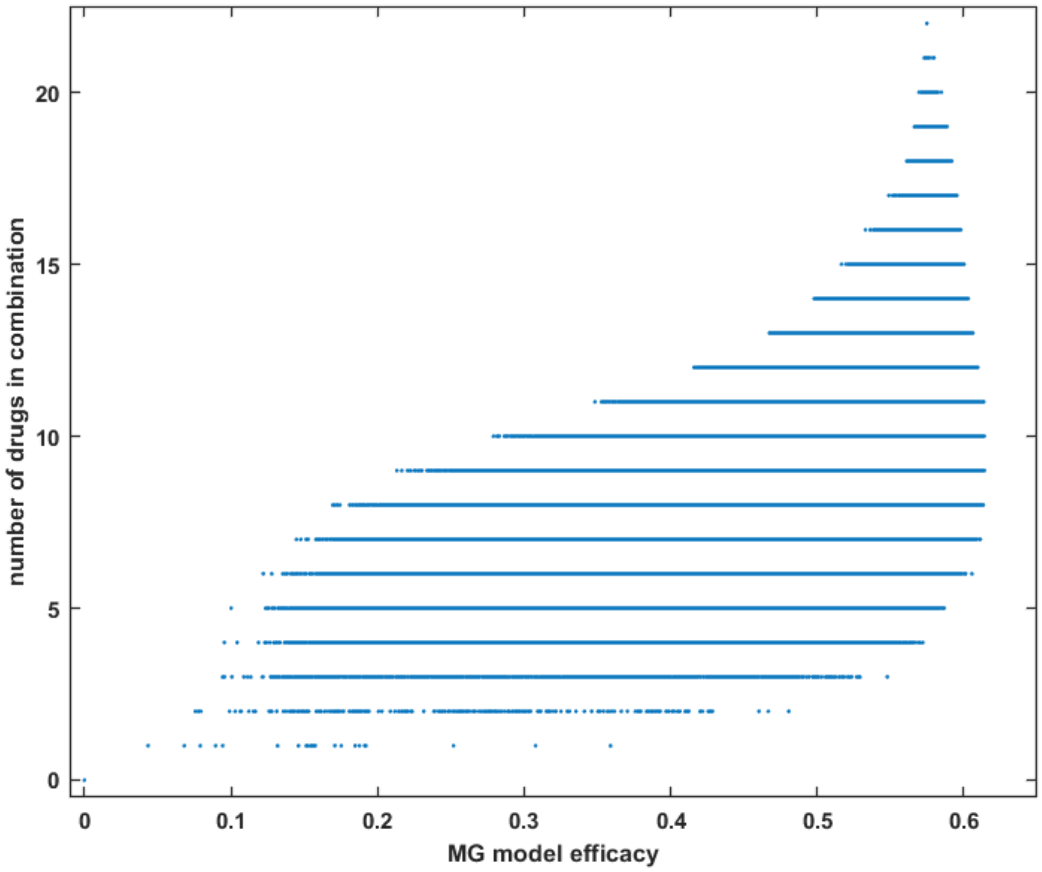

Fig. S5. Number of drugs in combination vs efficacy for the MG model. The MG model actually screens all 4,194,304 combinations of 22 drugs because the model has 1 drug representing each of 18 RADC drug categories, but has 2 drugs representing the antibiotic and antidiabetic drug categories (in the cases of 2 representative drugs per category the modeling results are averaged to give the mode response for that category). Each dot represents 1 of the 4,194,304 drug combinations, and the dots are arranged in horizontal rows according to the number of drugs in the combination (there are so many combinations that most of the dots run together into seemingly solid lines). Efficacy can range broadly for combinations composed of the same number of drugs. Maximal efficacy rises for combinations up to about seven drugs but then it levels off and even decreases as the number of drugs per combination continues to rise. This suggests that the model is capturing possible antagonistic interactions that would decrease the anti-inflammatory effect of individual drugs, even though it is trained mainly on drugs that have an anti-inflammatory effect by themselves.

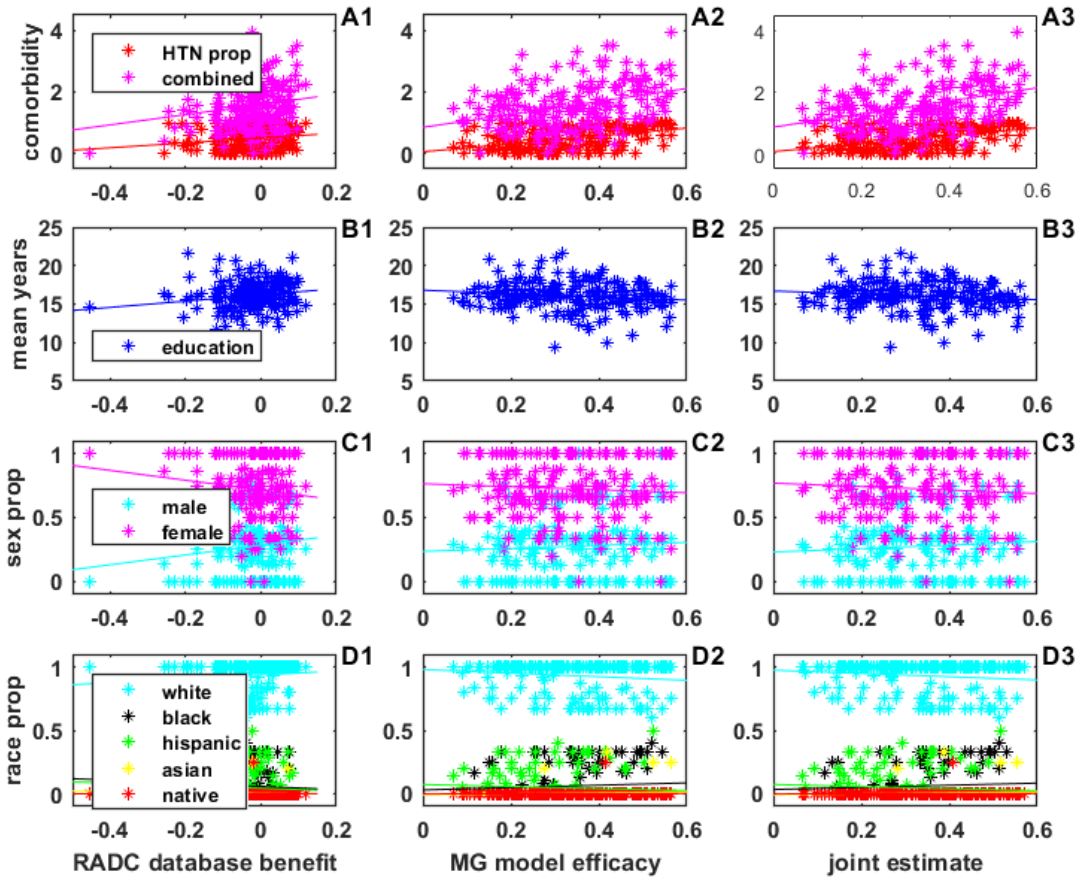

Fig. S6. Relationships between demographic variables and benefits/efficacies. Comorbidity, whether hypertension (HTN) specifically or combined comorbidity, is strongly positively correlated with the benefit/efficacy of drug combinations as determined from RADC alone, MG alone, or from MG and RADC jointly (A1, A2, and A3). The correlations between HTN or comorbidity and RADC benefit (A1) are only marginally significant. Education is positively correlated with RADC benefit (B1) but again significance is marginal. No other correlations are statistically significant. See Tabs. S6-S8 for numerical values associated with these regression analyses.

Tab. S4. Regression analyses of demographic variables and RADC benefit. Numerical results are for regression analyses of the demographic variables associated with the participants in the correlation set. The number of data points for all regression analyses reported in this table is 196. The row letters/numbers correspond to the panel letters/numbers in Fig. S6. HTN stands for hypertension. Comorbidity is combined comorbidity.

row (panel in Fig S6)	**relationship examined**	**slope of regression line**	**correlation coefficient**	**p-value for regression**
A1	HTN proportion vs RADC benefit	0.7929	0.1803	0.0114
A1	comorbidity vs RADC benefit	1.6601	0.1806	0.0113
B1	education vs RADC benefit	4.0465	0.1747	0.0143
C1	male proportion vs RADC benefit	0.3836	0.1335	0.0622
C1	female proportion vs RADC benefit	−0.3836	−0.1335	0.0622
D1	white proportion vs RADC benefit	0.1537	0.1016	0.1563
D1	black proportion vs RADC benefit	−0.1223	−0.0835	0.2445
D1	hispanic proportion vs RADC benefit	−0.0992	−0.0763	0.2880
D1	asian proportion vs RADC benefit	−0.0330	−0.0705	0.3263
D1	native proportion vs RADC benefit	0.0017	0.0075	0.9174

Tab. S5. Regression analyses of demographic variables and MG efficacy. Numerical results are for regression analyses of the demographic variables associated with the participants in the correlation set. The number of data points for all regression analyses reported in this table is 196. The row letters/numbers correspond to the panel letters/numbers in Fig. S6. HTN stands for hypertension. Comorbidity is combined comorbidity.

row (panel in Fig S6)	relationship examined	slope of regression line	correlation coefficient	p-value for regression
A2	HTN proportion vs MG efficacy	1.2812	0.4493	0.0000
A2	comorbidity vs MG efficacy	2.1050	0.3532	0.0000
B2	education vs MG efficacy	-2.1665	-0.1442	0.0437
C2	male proportion vs MG efficacy	0.1179	0.0633	0.3782
C2	female proportion vs MG efficacy	-0.1179	-0.0633	0.3782
D2	white proportion vs MG efficacy	-0.1411	-0.1440	0.0441
D2	black proportion vs MG efficacy	0.0935	0.0984	0.1700
D2	hispanic proportion vs MG efficacy	-0.0802	-0.0951	0.1848
D2	asian proportion vs MG efficacy	0.0408	0.1342	0.0607
D2	native proportion vs MG efficacy	0.0069	0.0474	0.5091

Tab. S6. Regression analyses of demographic variables and joint MG/RADC efficacy. Numerical results are for regression analyses of the demographic variables associated with the participants in the correlation set. The number of data points for all regression analyses reported in this table is 196. The row letters/numbers correspond to the panel letters/numbers in Fig. S6. HTN stands for hypertension. Comorbidity is combined comorbidity.

row (panel in Fig. S6)	**relationship examined**	**slope of regression line**	**correlation coefficient**	**p-value for regression**
A3	HTN proportion vs joint estimate	1.2821	0.4551	0.0000
A3	comorbidity vs joint estimate	2.1258	0.3611	0.0000
B3	education vs joint estimate	−1.8747	−0.1264	0.0776
C3	male proportion vs joint estimate	0.1349	0.0733	0.3073
C3	female proportion vs joint estimate	−0.1349	−0.0733	0.3073
D3	white proportion vs joint estimate	−0.1281	−0.1323	0.0645
D3	black proportion vs joint estimate	0.0837	0.0892	0.2135
D3	hispanic proportion vs joint estimate	−0.0829	−0.0996	0.1649
D3	asian proportion vs joint estimate	0.0376	0.1254	0.0798
D3	native proportion vs joint estimate	0.0068	0.0471	0.5124

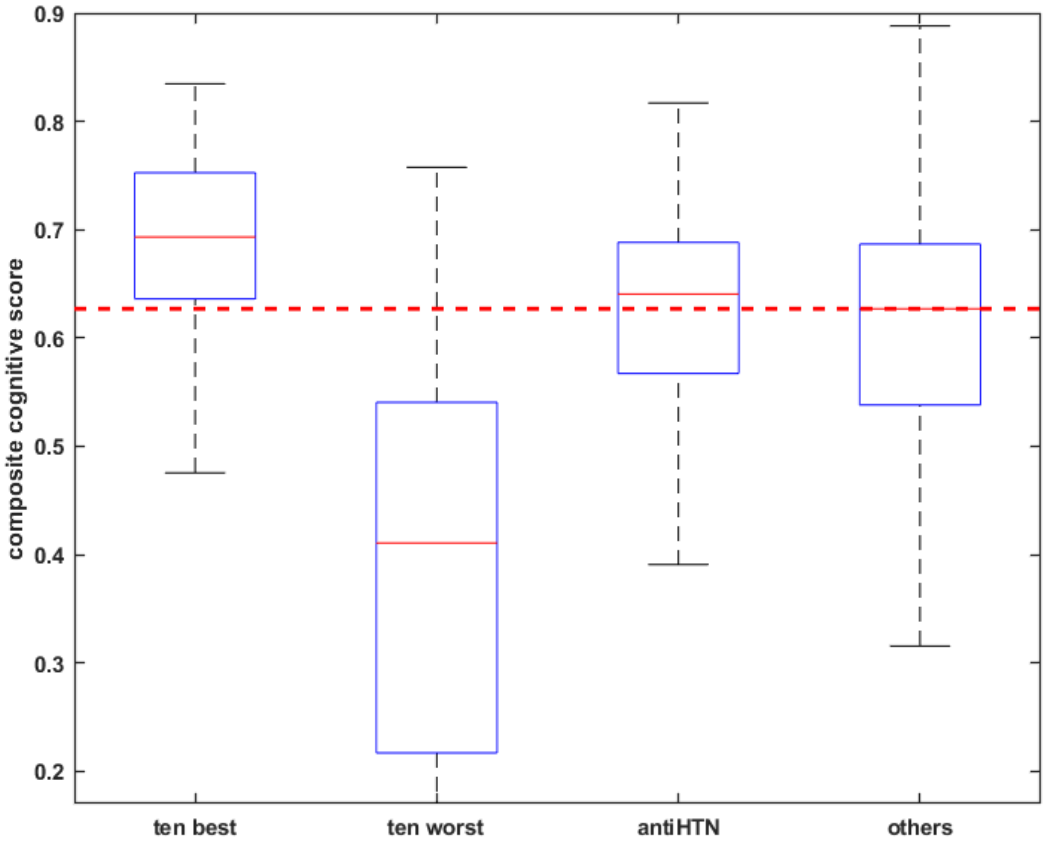

Fig. S7. Median cognitive scores for RADC-alone determined drug combinations. The plot shows the composite cognitive scores for the ten best and ten worst RADC-alone determined drug combinations, each taken as a whole group. Also shown are the median composite cognitive scores for the group of combinations of antihypertensive (antiHTN) medications along with COX2 inhibitors and aspirin, and those for all other drug combinations including the null (no-drug) combination. The antiHTN combinations are listed in Tab. S9. The central line in each box is the median, and the dashed line extending across the plot corresponds to the median for all other drug combinations including the null (no-drug) combination. The bottom of each box is the 25th percentile, the top is the 75th percentile, and the whiskers cover approximately 99% of all of the data points. The means of the ten best, ten worst, and antiHTN groups are all significantly different from the mean of the other group at the $p = 0.01$ level using the Bonferroni correction for multiple comparisons. Grouping the ten best, ten worst, and antiHTN combinations together was necessary in order to determine interaction probabilities using N-way ANOVA because not all combinations of factors were available when each drug combination was treated individually. The results of the N-way ANOVA analysis of the RADC-alone determined combinations is shown in Tab. S7.

Tab. S7. Factor interactions for RADC-alone determined drug combinations. The drug combinations are grouped into four levels as described in the caption to Fig. S7. Some main effects and some interactions are significant. Factor abbreviations are: drug4, the four drug combination groupings; comor, combined comorbidity score; HTN, hypertension; and educ, education.

Source	Sum Sq.	d.f.	Mean Sq.	F	Prob>F
drug4	0.219	3	0.07285	4.17	0.0059
age	0.116	1	0.1163	6.65	0.0099
comor	0.001	1	0.00139	0.08	0.7779
HTN	0.094	1	0.09378	5.36	0.0206
educ	1.653	1	1.65289	94.51	0
sex	0.065	1	0.06491	3.71	0.054
drug4*age	0.369	3	0.12304	7.04	0.0001
drug4*comor	0.419	3	0.13963	7.98	0
drug4*HTN	0.498	3	0.16614	9.5	0
drug4*educ	0.215	3	0.07161	4.09	0.0065
drug4*sex	0.171	3	0.05696	3.26	0.0206
age*comor	0.006	1	0.00628	0.36	0.5491
age*HTN	0	1	0.00047	0.03	0.87
age*educ	0.887	1	0.8871	50.72	0
age*sex	0.268	1	0.26837	15.34	0.0001
comor*HTN	0.79	1	0.7904	45.19	0
comor*educ	0.201	1	0.20112	11.5	0.0007
comor*sex	0.247	1	0.24721	14.14	0.0002
HTN*educ	0.002	1	0.00196	0.11	0.7381
HTN*sex	0.343	1	0.3429	19.61	0
educ*sex	0.272	1	0.27218	15.56	0.0001
Error	447.324	25577	0.01749		
Total	568.846	25610			

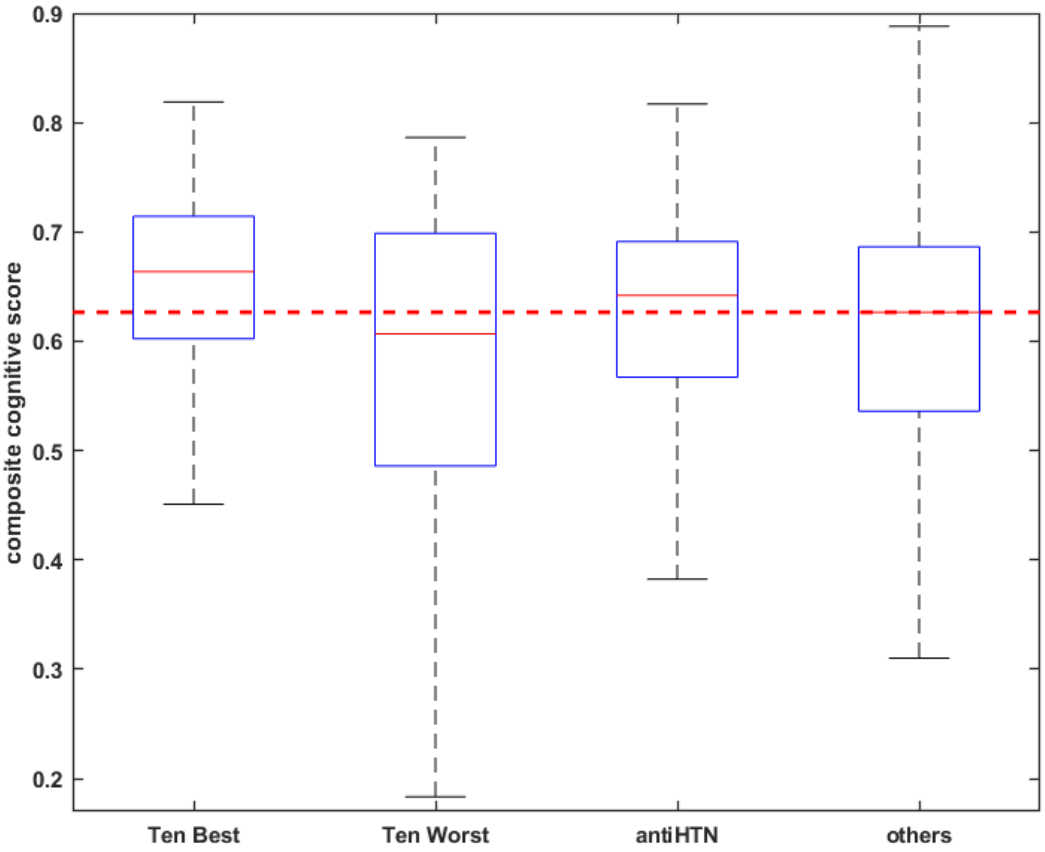

Fig. S8. Median cognitive scores for jointly determined drug combinations. The plot shows the composite cognitive scores for the Ten Best and Ten Worst jointly determined drug combinations, each taken as a whole group. Also shown are the median composite cognitive scores for the group of combinations of antiHTN medications along with COX2 inhibitors and aspirin, and those for all other drug combinations including the null (no-drug) combination. The antiHTN combinations are listed in Tab. S10. The central line in each box is the median, and the dashed line extending across the plot corresponds to the median for all other drug combinations including the null (no-drug) combination. The bottom of each box is the 25th percentile, the top is the 75th percentile, and the whiskers cover approximately 99% of all of the data points. The means of the Ten Best, Ten Worst, and antiHTN groups are all significantly different from the mean of the other group at the p = 0.01 level using the Bonferroni correction for multiple comparisons. Grouping the Ten Best, Ten Worst, and antiHTN combinations together was necessary in order to determine interaction probabilities using N-way ANOVA because not all combinations of factors were available when each drug combination was treated individually. The results of the N-way ANOVA analysis of the jointly determined combinations is shown in Tab. S8.

Tab. S8. Factor interactions for jointly (MG and RADC) determined drug combinations. The drug combinations are grouped into four levels as described in the caption to Fig. S8. Some main effects and some interactions are significant. Whereas the interaction between the drug combination groupings and hypertension was significant for the RADC-alone determined drug combinations (Tab. S7), it was not significant here for the jointly determined drug combinations. Factor abbreviations as in Tab. S7.

Source	Sum Sq.	d.f.	Mean Sq.	F	Prob>F
drug4	1.358	3	0.4525	25.25	0
age	0.096	1	0.09579	5.35	0.0208
comor	0.045	1	0.0449	2.51	0.1135
HTN	0.001	1	0.00143	0.08	0.7774
educ	1.772	1	1.77209	98.89	0
sex	0.163	1	0.16305	9.1	0.0026
drug4*age	0.741	3	0.24694	13.78	0
drug4*comor	0.876	3	0.29216	16.3	0
drug4*HTN	0.079	3	0.02649	1.48	0.2182
drug4*educ	0.742	3	0.24723	13.8	0
drug4*sex	0.082	3	0.02722	1.52	0.2072
age*comor	0.027	1	0.0268	1.5	0.2214
age*HTN	0	1	0.00001	0	0.9831
age*educ	0.758	1	0.75803	42.3	0
age*sex	0.338	1	0.33766	18.84	0
comor*HTN	0.786	1	0.7862	43.87	0
comor*educ	0.221	1	0.22068	12.31	0.0005
comor*sex	0.222	1	0.22228	12.4	0.0004
HTN*educ	0.007	1	0.00721	0.4	0.526
HTN*sex	0.184	1	0.1844	10.29	0.0013
educ*sex	0.156	1	0.15558	8.68	0.0032
Error	458.335	25577	0.01792		
Total	568.846	25610			

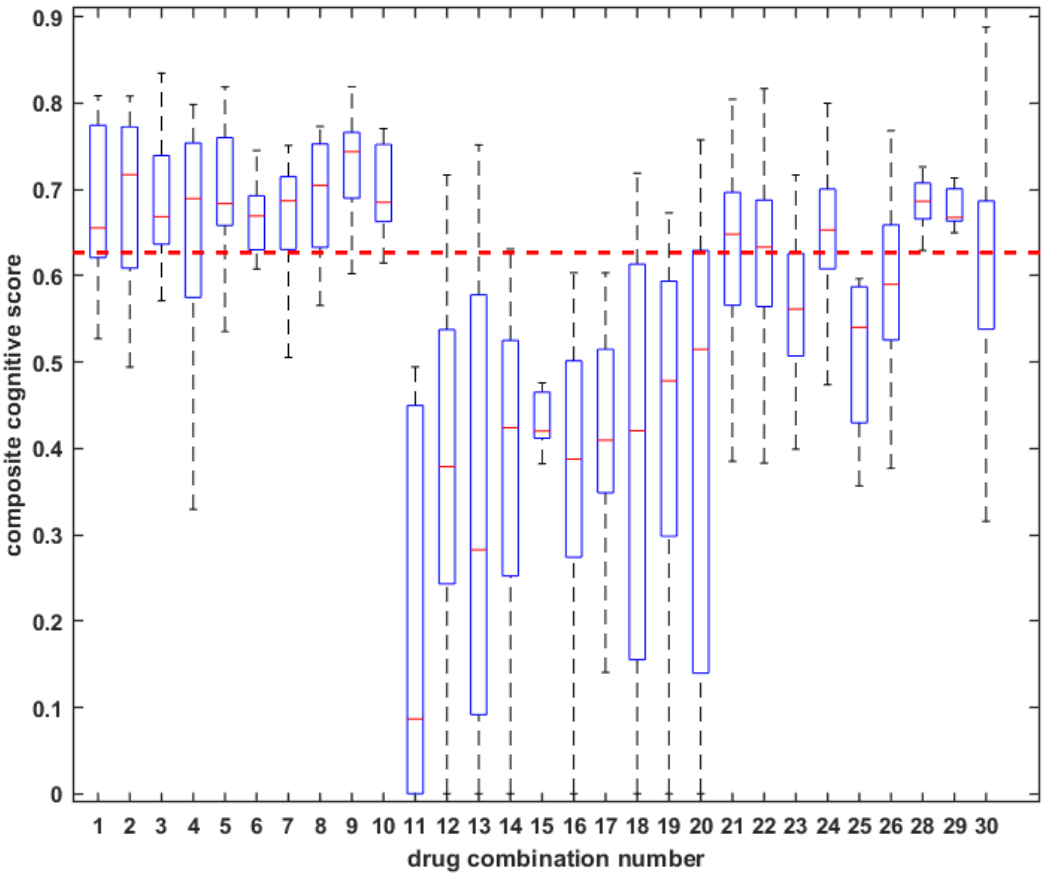

Fig. S9. Median cognitive scores for RADC-alone determined drug combinations. The plot shows the composite cognitive scores for the ten best and ten worst RADC-alone determined drug combinations, each taken individually. Also shown are the median composite cognitive scores for each of a set of combinations of antihypertensive (antiHTN) medications along with COX2 inhibitors and aspirin, and those for all other drug combinations including the null (no-drug) combination. The antiHTN combinations are listed in Tab. S9. Note that the seventh antiHTN combination (number 27) is excluded from this plot because it is the same as the fourth best combination (number 4). The central line is each box is the median, and the dashed line extending across the plot corresponds to the median for all other drug combinations including the null (no-drug) combination. The bottom of each box is the 25th percentile, the top is the 75th percentile, and the whiskers cover approximately 99% of all of the data points. The medians for the ten best combinations (numbers 1-10) and for the ten worst combinations (numbers 11-20) all are, respectively, higher and lower than the median for all other drug combinations (number 30). This demonstrates agreement between the RADC dataset benefit measurement, which was used to determine the ten best and worst, and statistics based on the composite cognitive score directly. The means and sample sizes for all drug combinations are shown in Tab. S9.

Tab. S9. Means and sample sizes for RADC-alone determined drug combinations. This table includes the ten best and the ten worst RADC-alone determined drug combinations. It also includes a set of combinations of a COX2 inhibitor (COX2I) and aspirin and the antihypertensive (antiHTN) drug classes of ACE inhibitor (ACEI), beta blocker (BB), calcium channel blocker (CCB), and angiotensin-receptor blocker (ARB). Note that the combination of aspirin, ACEI, BB, CCB, and ARB is the same as combination 4 of the ten best RADC-alone determined drug combinations. The last entry is for all other combinations including the null (no-drug) combination. The main effect of drug combination is significant at $p = 3.1415 \times 10^{-137}$. Means in boldface are significant at the $p = 0.01$ level using the Bonferroni correction for multiple comparisons with the last entry.

Drug combination	Factor name	Mean	Sample size
1	combination 1 of ten best	0.6876	30
2	combination 2 of ten best	0.6903	34
3	combination 3 of ten best	0.6926	26
4	combination 4 of ten best	0.6678	23
5	combination 5 of ten best	**0.6992**	57
6	combination 6 of ten best	0.6669	22
7	combination 7 of ten best	0.6570	36
8	combination 8 of ten best	0.6861	32
9	combination 9 of ten best	**0.7291**	39
10	combination 10 of ten best	0.6977	17
11	combination 1 of ten worst	**0.2042**	16
12	combination 2 of ten worst	**0.3830**	44
13	combination 3 of ten worst	**0.3299**	23
14	combination 4 of ten worst	**0.3723**	27
15	combination 5 of ten worst	0.4316	8
16	combination 6 of ten worst	**0.3567**	26
17	combination 7 of ten worst	**0.4049**	29
18	combination 8 of ten worst	**0.3911**	39
19	combination 9 of ten worst	**0.4242**	46
20	combination 10 of ten worst	**0.4032**	23
21	COX2 inhibitor (COX2I) alone	0.6102	75
22	aspirin alone	0.6067	282
23	calcium channel blocker (CCB) alone	0.5566	27
24	COX2I and aspirin	0.6421	146
25	COX2I and CCB	0.5084	4
26	aspirin and CCB	0.5928	62
27	COX2I, aspirin, and CCB	0.6678	23
28	aspirin, ACE inhibitor (ACEI), beta blocker (BB), CCB, and angiotensin receptor blocker (ARB)	0.6861	14
29	COX2I, aspirin, ACEI, BB, CCB, and ARB	0.6792	15
30	all other combinations including null (no-drug) combination	0.5890	24,737

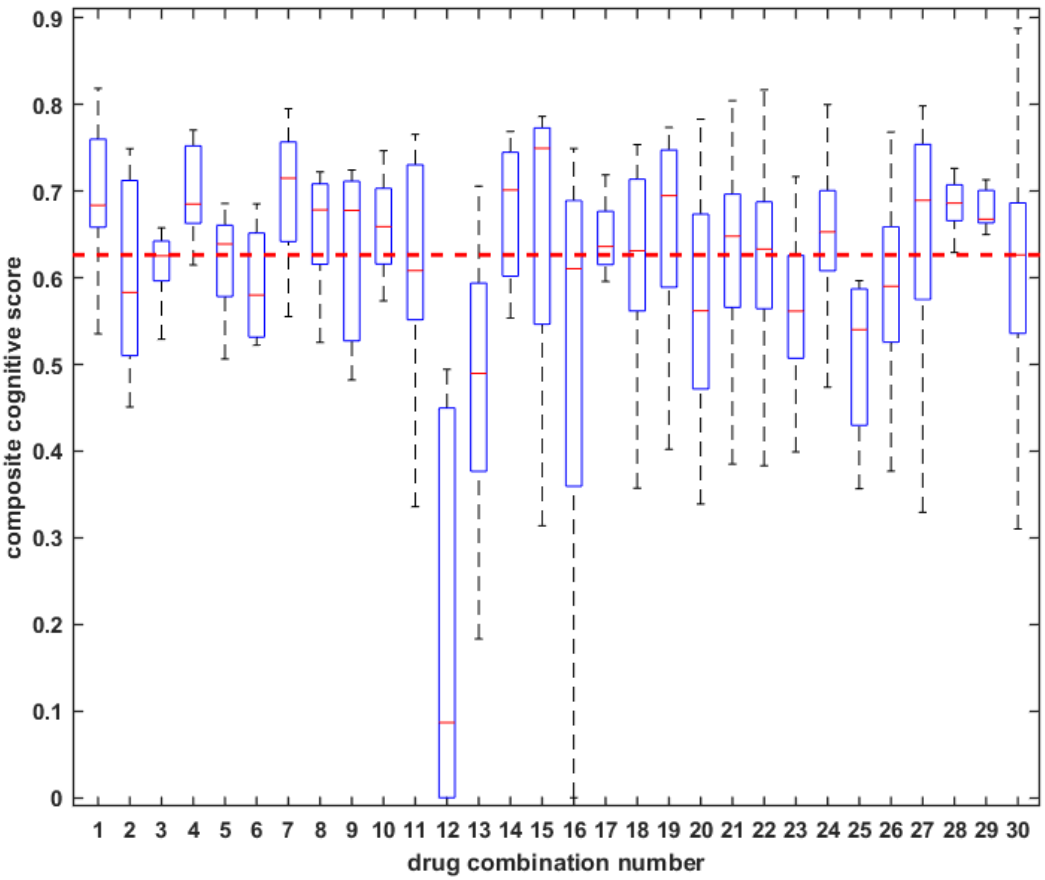

Fig. S10. Median cognitive scores for jointly determined drug combinations. The plot shows the composite cognitive scores for the Ten Best and Ten Worst jointly determined drug combinations, each taken individually. Also shown are the median composite cognitive scores for each of a set of combinations of antihypertensive (antiHTN) medications along with COX2 inhibitors and aspirin, and those for all other drug combinations including the null combination. The antiHTN combinations are listed in Tab. S10. The central line is each box is the median, and the dashed line extending across the plot corresponds to the median for all other drug combinations including the null (no-drug) combination. The bottom of each box is the 25th percentile, the top is the 75th percentile, and the whiskers cover approximately 99% of all of the data points. The medians for the Ten Best combinations (numbers 1-10) and for the Ten Worst combinations (numbers 11-20) not all are, respectively, higher and lower than the median for all other drug combinations (number 30), and this reflects the discrepancies between the MG model efficacies and the RADC benefits that are apparent in the correlation shown in Fig. 1 of the main text. The means and sample sizes for all drug combinations are shown in Tab. S10.

Tab. S10. Means and sample sizes for jointly determined drug combinations. This table included the Ten Best and the Ten Worst jointly determined drug combinations. It also includes a set of combinations of a COX2 inhibitor (COX2I) and aspirin and the antihypertensive (antiHTN) drug classes of ACE inhibitor (ACEI), beta blocker (BB), calcium channel blocker (CCB), and angiotensin-receptor blocker (ARB). The data for the COX2I/aspirin/antiHTN combinations are the same as in Tab. S9. The last entry is for all other combinations including the null (no-drug) combination. The main effect of drug combination (with jointly determined Ten Best and Ten Worst) is significant at $p = 5.7818^{-44}$. Means in boldface are significant at the p = 0.01 level using the Bonferroni correction for multiple comparisons with the last entry.

Drug combination	Factor name	Mean	Sample size
1	combination 1 of Ten Best	**0.6992**	57
2	combination 2 of Ten Best	0.5789	33
3	combination 3 of Ten Best	0.5896	22
4	combination 4 of Ten Best	0.6977	17
5	combination 5 of Ten Best	0.6136	26
6	combination 6 of Ten Best	0.6080	20
7	combination 7 of Ten Best	**0.6954**	52
8	combination 8 of Ten Best	0.6568	21
9	combination 9 of Ten Best	0.6329	23
10	combination 10 of Ten Best	0.6621	30
11	combination 1 of Ten Worst	0.6153	52
12	combination 2 of Ten Worst	**0.2042**	16
13	combination 3 of Ten Worst	**0.4736**	54
14	combination 4 of Ten Worst	0.6521	28
15	combination 5 of Ten Worst	0.6626	21
16	combination 6 of Ten Worst	0.5039	55
17	combination 7 of Ten Worst	0.6471	15
18	combination 8 of Ten Worst	0.6045	30
19	combination 9 of Ten Worst	0.6418	26
20	combination 10 of Ten Worst	0.5420	26
21	COX2 inhibitor (COX2I) alone	0.6102	75
22	aspirin alone	0.6067	282
23	calcium channel blocker (CCB) alone	0.5566	27
24	COX2I and aspirin	0.6421	146
25	COX2I and CCB	0.5084	4
26	aspirin and CCB	0.5928	62
27	COX2I, aspirin, and CCB	0.6678	23
28	aspirin, ACE inhibitor (ACEI), beta blocker (BB), CCB, and angiotensin receptor blocker (ARB)	0.6861	14
29	COX2I, aspirin, ACEI, BB, CCB, and ARB	0.6792	15
30	all other combinations including null (no-drug) combination	0.5874	24,687

References

[1] Kim H, Bae S, Kwon KY, Hwang YI, Kang JS, Lee WJ (2015) A combinational effect of acetaminophen and oriental herbs on the regulation of inflammatory mediators in microglia cell line, BV2. *Anat Cell Biol* **48**, 244-250.

[2] Pettit LK, Varsanyi C, Tadros J, Vassiliou E (2013) Modulating the inflammatory properties of activated microglia with Docosahexaenoic acid and Aspirin. *Lipids Health Dis* **12**, 16.

[3] Yang JM, Rui BB, Chen C, Chen H, Xu TJ, Xu WP, Wei W (2014) Acetylsalicylic acid enhances the anti-inflammatory effect of fluoxetine through inhibition of NF-kappaB, p38-MAPK and ERK1/2 activation in lipopolysaccharide-induced BV-2 microglia cells. *Neuroscience* **275**, 296-304.

[4] Rocha SM, Saraiva T, Cristovao AC, Ferreira R, Santos T, Esteves M, Saraiva C, Je G, Cortes L, Valero J, Alves G, Klibanov A, Kim YS, Bernardino L (2016) Histamine induces microglia activation and dopaminergic neuronal toxicity via H1 receptor activation. *J Neuroinflammation* **13**, 137.

[5] Mori K, Ozaki E, Zhang B, Yang L, Yokoyama A, Takeda I, Maeda N, Sakanaka M, Tanaka J (2002) Effects of norepinephrine on rat cultured microglial cells that express alpha1, alpha2, beta1 and beta2 adrenergic receptors. *Neuropharmacology* **43**, 1026-1034.

[6] Lee YJ, Choi DY, Choi IS, Han JY, Jeong HS, Han SB, Oh KW, Hong JT (2011) Inhibitory effect of a tyrosine-fructose Maillard reaction product, 2,4-bis(p-hydroxyphenyl)-2-butenal on amyloid-beta generation and inflammatory reactions via inhibition of NF-kappaB and STAT3 activation in cultured astrocytes and microglial BV-2 cells. *J Neuroinflammation* **8**, 132.

[7] Kim JA, Yun HM, Jin P, Lee HP, Han JY, Udumula V, Moon DC, Han SB, Oh KW, Ham YW, Jung HS, Song HS, Hong JT (2014) Inhibitory effect of a 2,4-bis(4-hydroxyphenyl)-2-butenal diacetate on neuro-inflammatory reactions via inhibition of STAT1 and STAT3 activation in cultured astrocytes and microglial BV-2 cells. *Neuropharmacology* **79**, 476-487.

[8] Kang CH, Jayasooriya RG, Dilshara MG, Choi YH, Jeong YK, Kim ND, Kim GY (2012) Caffeine suppresses lipopolysaccharide-stimulated BV2 microglial cells by suppressing Akt-mediated NF-kappaB activation and ERK phosphorylation. *Food Chem Toxicol* **50**, 4270-4276.

[9] Chantong B, Kratschmar DV, Nashev LG, Balazs Z, Odermatt A (2012) Mineralocorticoid and glucocorticoid receptors differentially regulate NF-kappaB activity and pro-inflammatory cytokine production in murine BV-2 microglial cells. *J Neuroinflammation* **9**, 260.

[10] Taneo J, Adachi T, Yoshida A, Takayasu K, Takahara K, Inaba K (2015) Amyloid beta oligomers induce interleukin-1beta production in primary microglia in a cathepsin B- and reactive oxygen species-dependent manner. *Biochem Biophys Res Commun* **458**, 561-567.

[11] Koch MW, Zabad R, Giuliani F, Hader W, Jr., Lewkonia R, Metz L, Wee Yong V (2015) Hydroxychloroquine reduces microglial activity and attenuates experimental autoimmune encephalomyelitis. *J Neurol Sci* **358**, 131-137.

[12] Ishii Y, Yamaizumi A, Kawakami A, Islam A, Choudhury ME, Takahashi H, Yano H, Tanaka J (2015) Anti-inflammatory effects of noradrenaline on LPS-treated microglial cells: Suppression of NFkappaB nuclear translocation and subsequent STAT1 phosphorylation. *Neurochem Int* **90**, 56-66.

[13] Han Y, Jiang C, Tang J, Wang C, Wu P, Zhang G, Liu W, Jamangulova N, Wu X, Song X (2014) Resveratrol reduces morphine tolerance by inhibiting microglial activation via AMPK signalling. *Eur J Pain* **18**, 1458-1470.

[14] Pan Y, Sun X, Jiang L, Hu L, Kong H, Han Y, Qian C, Song C, Qian Y, Liu W (2016) Metformin reduces morphine tolerance by inhibiting microglial-mediated neuroinflammation. *J Neuroinflammation* **13**, 294.

[15] Chao CC, Hu S, Close K, Choi CS, Molitor TW, Novick WJ, Peterson PK (1992) Cytokine release from microglia: differential inhibition by pentoxifylline and dexamethasone. *J Infect Dis* **166**, 847-853.

[16] Wilms H, Sievers J, Rickert U, Rostami-Yazdi M, Mrowietz U, Lucius R (2010) Dimethylfumarate inhibits microglial and astrocytic inflammation by suppressing the synthesis of nitric oxide, IL-1beta, TNF-alpha and IL-6 in an in-vitro model of brain inflammation. *J Neuroinflammation* **7**, 30.

[17] Dong H, Zhang W, Zeng X, Hu G, Zhang H, He S, Zhang S (2014) Histamine induces upregulated expression of histamine receptors and increases release of inflammatory mediators from microglia. *Mol Neurobiol* **49**, 1487-1500.

[18] Zhu J, Qu C, Lu X, Zhang S (2014) Activation of microglia by histamine and substance P. *Cell Physiol Biochem* **34**, 768-780.

[19] Pawate S, Shen Q, Fan F, Bhat NR (2004) Redox regulation of glial inflammatory response to lipopolysaccharide and interferongamma. *J Neurosci Res* **77**, 540-551.

[20] Zhao S, Zhang L, Lian G, Wang X, Zhang H, Yao X, Yang J, Wu C (2011) Sildenafil attenuates LPS-induced pro-inflammatory responses through down-regulation of intracellular ROS-related MAPK/NF-kappaB signaling pathways in N9 microglia. *Int Immunopharmacol* **11**, 468-474.

[21] Lijia Z, Zhao S, Wang X, Wu C, Yang J (2012) A self-propelling cycle mediated by reactive oxide species and nitric oxide exists in LPS-activated microglia. *Neurochem Int* **61**, 1220-1230.

[22] Yuan Y, Zha H, Rangarajan P, Ling EA, Wu C (2014) Anti-inflammatory effects of Edaravone and Scutellarin in activated microglia in experimentally induced ischemia injury in rats and in BV-2 microglia. *BMC Neurosci* **15**, 125.

[23] Zhao TZ, Ding Q, Hu J, He SM, Shi F, Ma LT (2016) GPER expressed on microglia mediates the anti-inflammatory effect of estradiol in ischemic stroke. *Brain Behav* **6**, e00449.

[24] Morsali D, Bechtold D, Lee W, Chauhdry S, Palchaudhuri U, Hassoon P, Snell DM, Malpass K, Piers T, Pocock J, Roach A, Smith KJ (2013) Safinamide and flecainide protect axons and reduce microglial activation in models of multiple sclerosis. *Brain* **136**, 1067-1082.

[25] Liu D, Wang Z, Liu S, Wang F, Zhao S, Hao A (2011) Anti-inflammatory effects of fluoxetine in lipopolysaccharide(LPS)-stimulated microglial cells. *Neuropharmacology* **61**, 592-599.

[26] Su F, Yi H, Xu L, Zhang Z (2015) Fluoxetine and S-citalopram inhibit M1 activation and promote M2 activation of microglia in vitro. *Neuroscience* **294**, 60-68.

[27] Ingham V, Williams A, Bate C (2014) Glimepiride reduces CD14 expression and cytokine secretion from macrophages. *J Neuroinflammation* **11**, 115.

[28] Lim GP, Yang F, Chu T, Chen P, Beech W, Teter B, Tran T, Ubeda O, Ashe KH, Frautschy SA, Cole GM (2000) Ibuprofen suppresses plaque pathology and inflammation in a mouse model for Alzheimer's disease. *J Neurosci* **20**, 5709-5714.

[29] Yan Q, Zhang J, Liu H, Babu-Khan S, Vassar R, Biere AL, Citron M, Landreth G (2003) Anti-inflammatory drug therapy alters beta-amyloid processing and deposition in an animal model of Alzheimer's disease. *J Neurosci* **23**, 7504-7509.

[30] Wilkinson BL, Cramer PE, Varvel NH, Reed-Geaghan E, Jiang Q, Szabo A, Herrup K, Lamb BT, Landreth GE (2012) Ibuprofen attenuates oxidative damage through NOX2 inhibition in Alzheimer's disease. *Neurobiol Aging* **33**, 197 e121-132.

[31] Aloisi F, Penna G, Cerase J, Menendez Iglesias B, Adorini L (1997) IL-12 production by central nervous system microglia is inhibited by astrocytes. *J Immunol* **159**, 1604-1612.

[32] Minghetti L, Nicolini A, Polazzi E, Creminon C, Maclouf J, Levi G (1997) Inducible nitric oxide synthase expression in activated rat microglial cultures is downregulated by exogenous prostaglandin E2 and by cyclooxygenase inhibitors. *Glia* **19**, 152-160.

[33] Aloisi F, De Simone R, Columba-Cabezas S, Levi G (1999) Opposite effects of interferon-gamma and prostaglandin E2 on tumor necrosis factor and interleukin-10 production in microglia: a regulatory loop controlling microglia pro- and anti-inflammatory activities. *J Neurosci Res* **56**, 571-580.

[34] Correa F, Hernangomez M, Mestre L, Loria F, Spagnolo A, Docagne F, Di Marzo V, Guaza C (2010) Anandamide enhances IL-10 production in activated microglia by targeting CB(2) receptors: roles of ERK1/2, JNK, and NF-kappaB. *Glia* **58**, 135-147.

[35] Ehrhart J, Obregon D, Mori T, Hou H, Sun N, Bai Y, Klein T, Fernandez F, Tan J, Shytle RD (2005) Stimulation of cannabinoid receptor 2 (CB2) suppresses microglial activation. *J Neuroinflammation* **2**, 29.

[36] Wang YP, Wu Y, Li LY, Zheng J, Liu RG, Zhou JP, Yuan SY, Shang Y, Yao SL (2011) Aspirin-triggered lipoxin A4 attenuates LPS-induced pro-inflammatory responses by inhibiting activation of NF-kappaB and MAPKs in BV-2 microglial cells. *J Neuroinflammation* **8**, 95.

[37] Dong H, Zhang X, Dai X, Lu S, Gui B, Jin W, Zhang S, Zhang S, Qian Y (2014) Lithium ameliorates lipopolysaccharide-induced microglial activation via inhibition of toll-like receptor 4 expression by activating the PI3K/Akt/FoxO1 pathway. *J Neuroinflammation* **11**, 140.

[38] Khan MS, Ali T, Abid MN, Jo MH, Khan A, Kim MW, Yoon GH, Cheon EW, Rehman SU, Kim MO (2017) Lithium ameliorates lipopolysaccharide-induced neurotoxicity in the cortex and hippocampus of the adult rat brain. *Neurochem Int* **108**, 343-354.

[39] Xie Z, Wei M, Morgan TE, Fabrizio P, Han D, Finch CE, Longo VD (2002) Peroxynitrite mediates neurotoxicity of amyloid beta-peptide1-42- and lipopolysaccharide-activated microglia. *J Neurosci* **22**, 3484-3492.

[40] Miyoshi M, Miyano K, Moriyama N, Taniguchi M, Watanabe T (2008) Angiotensin type 1 receptor antagonist inhibits lipopolysaccharide-induced stimulation of rat microglial cells by suppressing nuclear factor kappaB and activator protein-1 activation. *Eur J Neurosci* **27**, 343-351.

[41] Benicky J, Sanchez-Lemus E, Honda M, Pang T, Orecna M, Wang J, Leng Y, Chuang DM, Saavedra JM (2011) Angiotensin II AT1 receptor blockade ameliorates brain inflammation. *Neuropsychopharmacology* **36**, 857-870.

[42] Bhat SA, Goel R, Shukla R, Hanif K (2016) Angiotensin Receptor Blockade Modulates NFkappaB and STAT3 Signaling and Inhibits Glial Activation and Neuroinflammation Better than Angiotensin-Converting Enzyme Inhibition. *Mol Neurobiol* **53**, 6950-6967.

[43] Torika N, Asraf K, Danon A, Apte RN, Fleisher-Berkovich S (2016) Telmisartan Modulates Glial Activation: In Vitro and In Vivo Studies. *PLoS One* **11**, e0155823.

[44] Hoppe JB, Frozza RL, Horn AP, Comiran RA, Bernardi A, Campos MM, Battastini AM, Salbego C (2010) Amyloid-beta neurotoxicity in organotypic culture is attenuated by melatonin: involvement of GSK-3beta, tau and neuroinflammation. *J Pineal Res* **48**, 230-238.

[45] Ionov M, Burchell V, Klajnert B, Bryszewska M, Abramov AY (2011) Mechanism of neuroprotection of melatonin against beta-amyloid neurotoxicity. *Neuroscience* **180**, 229-237.

[46] Park E, Chun HS (2017) Melatonin Attenuates Manganese and Lipopolysaccharide-Induced Inflammatory Activation of BV2 Microglia. *Neurochem Res* **42**, 656-666.

[47] Nikodemova M, Duncan ID, Watters JJ (2006) Minocycline exerts inhibitory effects on multiple mitogen-activated protein kinases and IkappaBalpha degradation in a stimulus-specific manner in microglia. *J Neurochem* **96**, 314-323.

[48] Kobayashi K, Imagama S, Ohgomori T, Hirano K, Uchimura K, Sakamoto K, Hirakawa A, Takeuchi H, Suzumura A, Ishiguro N, Kadomatsu K (2013) Minocycline selectively inhibits M1 polarization of microglia. *Cell Death Dis* **4**, e525.

[49] Wang X, Loram LC, Ramos K, de Jesus AJ, Thomas J, Cheng K, Reddy A, Somogyi AA, Hutchinson MR, Watkins LR, Yin H (2012) Morphine activates neuroinflammation in a manner parallel to endotoxin. *Proc Natl Acad Sci U S A* **109**, 6325-6330.

[50] Jiang C, Xu L, Chen L, Han Y, Tang J, Yang Y, Zhang G, Liu W (2015) Selective suppression of microglial activation by paeoniflorin attenuates morphine tolerance. *Eur J Pain* **19**, 908-919.

[51] Jiang X, Ni Y, Liu T, Zhang M, Ren H, Xu G (2013) Inhibition of LPS-induced retinal microglia activation by naloxone does not prevent photoreceptor death. *Inflammation* **36**, 42-52.

[52] Xu YF, Fu LL, Jiang CH, Qin YW, Ni YQ, Fan JW (2012) Naloxone inhibition of lipopolysaccharide-induced activation of retinal microglia is partly mediated via the p38 mitogen activated protein kinase signalling pathway. *J Int Med Res* **40**, 1438-1448.

[53] Shytle RD, Mori T, Townsend K, Vendrame M, Sun N, Zeng J, Ehrhart J, Silver AA, Sanberg PR, Tan J (2004) Cholinergic modulation of microglial activation by alpha 7 nicotinic receptors. *J Neurochem* **89**, 337-343.

[54] De Simone R, Ajmone-Cat MA, Carnevale D, Minghetti L (2005) Activation of alpha7 nicotinic acetylcholine receptor by nicotine selectively up-regulates cyclooxygenase-2 and prostaglandin E2 in rat microglial cultures. *J Neuroinflammation* **2**, 4.

[55] Moon JH, Kim SY, Lee HG, Kim SU, Lee YB (2008) Activation of nicotinic acetylcholine receptor prevents the production of reactive oxygen species in fibrillar beta amyloid peptide (1-42)-stimulated microglia. *Exp Mol Med* **40**, 11-18.

[56] Liu Y, Lo YC, Qian L, Crews FT, Wilson B, Chen HL, Wu HM, Chen SH, Wei K, Lu RB, Ali S, Hong JS (2011) Verapamil protects dopaminergic neuron damage through a novel anti-inflammatory mechanism by inhibition of microglial activation. *Neuropharmacology* **60**, 373-380.

[57] Huang BR, Chang PC, Yeh WL, Lee CH, Tsai CF, Lin C, Lin HY, Liu YS, Wu CY, Ko PY, Huang SS, Hsu HC, Lu DY (2014) Anti-neuroinflammatory effects of the calcium channel blocker nicardipine on microglial cells: implications for neuroprotection. *PLoS One* **9**, e91167.

[58] Espinosa-Parrilla JF, Martinez-Moreno M, Gasull X, Mahy N, Rodriguez MJ (2015) The L-type voltage-gated calcium channel modulates microglial pro-inflammatory activity. *Mol Cell Neurosci* **64**, 104-115.

[59] Hashioka S, Klegeris A, McGeer PL (2009) Proton pump inhibitors exert anti-inflammatory effects and decrease human microglial and monocytic THP-1 cell neurotoxicity. *Exp Neurol* **217**, 177-183.

[60] Torika N, Asraf K, Roasso E, Danon A, Fleisher-Berkovich S (2016) Angiotensin Converting Enzyme Inhibitors Ameliorate Brain Inflammation Associated with Microglial Activation: Possible Implications for Alzheimer's Disease. *J Neuroimmune Pharmacol* **11**, 774-785.

[61] af Forselles KJ, Root J, Clarke T, Davey D, Aughton K, Dack K, Pullen N (2011) In vitro and in vivo characterization of PF-04418948, a novel, potent and selective prostaglandin EP(2) receptor antagonist. *Br J Pharmacol* **164**, 1847-1856.

[62] Jiang J, Ganesh T, Du Y, Quan Y, Serrano G, Qui M, Speigel I, Rojas A, Lelutiu N, Dingledine R (2012) Small molecule antagonist reveals seizure-induced mediation of neuronal injury by prostaglandin E2 receptor subtype EP2. *Proc Natl Acad Sci U S A* **109**, 3149-3154.

[63] Jiang J, Quan Y, Ganesh T, Pouliot WA, Dudek FE, Dingledine R (2013) Inhibition of the prostaglandin receptor EP2 following status epilepticus reduces delayed mortality and brain inflammation. *Proc Natl Acad Sci U S A* **110**, 3591-3596.

[64] Chang JY, Liu LZ (2000) Catecholamines inhibit microglial nitric oxide production. *Brain Res Bull* **52**, 525-530.

[65] Colton CA (2009) Heterogeneity of microglial activation in the innate immune response in the brain. *J Neuroimmune Pharmacol* **4**, 399-418.

[66] Rojanathammanee L, Puig KL, Combs CK (2013) Pomegranate polyphenols and extract inhibit nuclear factor of activated T-cell activity and microglial activation in vitro and in a transgenic mouse model of Alzheimer disease. *J Nutr* **143**, 597-605.

[67] Olajide OA, Kumar A, Velagapudi R, Okorji UP, Fiebich BL (2014) Punicalagin inhibits neuroinflammation in LPS-activated rat primary microglia. *Mol Nutr Food Res* **58**, 1843-1851.

[68] Bi XL, Yang JY, Dong YX, Wang JM, Cui YH, Ikeshima T, Zhao YQ, Wu CF (2005) Resveratrol inhibits nitric oxide and TNF-alpha production by lipopolysaccharide-activated microglia. *Int Immunopharmacol* **5**, 185-193.

[69] Capiralla H, Vingtdeux V, Zhao H, Sankowski R, Al-Abed Y, Davies P, Marambaud P (2012) Resveratrol mitigates lipopolysaccharide- and Abeta-mediated microglial inflammation by inhibiting the TLR4/NF-kappaB/STAT signaling cascade. *J Neurochem* **120**, 461-472.

[70] Steiner N, Balez R, Karunaweera N, Lind JM, Munch G, Ooi L (2016) Neuroprotection of Neuro2a cells and the cytokine suppressive and anti-inflammatory mode of action of resveratrol in activated RAW264.7 macrophages and C8-B4 microglia. *Neurochem Int* **95**, 46-54.

[71] Bi W, Zhu L, Wang C, Liang Y, Liu J, Shi Q, Tao E (2011) Rifampicin inhibits microglial inflammation and improves neuron survival against inflammation. *Brain Res* **1395**, 12-20.

[72] Bi W, Zhu L, Jing X, Zeng Z, Liang Y, Xu A, Liu J, Xiao S, Yang L, Shi Q, Guo L, Tao E (2014) Rifampicin improves neuronal apoptosis in LPS-stimulated cocultured BV2 cells through inhibition of the TLR-4 pathway. *Mol Med Rep* **10**, 1793-1799.

[73] Heneka MT, Sastre M, Dumitrescu-Ozimek L, Hanke A, Dewachter I, Kuiperi C, O'Banion K, Klockgether T, Van Leuven F, Landreth GE (2005) Acute treatment with the PPARgamma agonist pioglitazone and ibuprofen reduces glial inflammation and Abeta1-42 levels in APPV717I transgenic mice. *Brain* **128**, 1442-1453.

[74] Loane DJ, Deighan BF, Clarke RM, Griffin RJ, Lynch AM, Lynch MA (2009) Interleukin-4 mediates the neuroprotective effects of rosiglitazone in the aged brain. *Neurobiol Aging* **30**, 920-931.

[75] Yamanaka M, Ishikawa T, Griep A, Axt D, Kummer MP, Heneka MT (2012) PPARgamma/RXRalpha-induced and CD36-mediated microglial amyloid-beta phagocytosis results in cognitive improvement in amyloid precursor protein/presenilin 1 mice. *J Neurosci* **32**, 17321-17331.

[76] Wang S, Wang H, Guo H, Kang L, Gao X, Hu L (2011) Neuroprotection of Scutellarin is mediated by inhibition of microglial inflammatory activation. *Neuroscience* **185**, 150-160.

[77] Nunes AK, Raposo C, Rocha SW, Barbosa KP, Luna RL, da Cruz-Hofling MA, Peixoto CA (2015) Involvement of AMPK, IKbetaalpha-NFkappaB and eNOS in the sildenafil anti-inflammatory mechanism in a demyelination model. *Brain Res* **1627**, 119-133.

[78] Fan H, Guo Y, Liang X, Yuan Y, Qi X, Wang M, Ma J, Zhou H (2013) Hydrogen sulfide protects against amyloid beta-peptide induced neuronal injury via attenuating inflammatory responses in a rat model. *J Biomed Res* **27**, 296-304.

[79] Craner MJ, Damarjian TG, Liu S, Hains BC, Lo AC, Black JA, Newcombe J, Cuzner ML, Waxman SG (2005) Sodium channels contribute to microglia/macrophage activation and function in EAE and MS. *Glia* **49**, 220-229.

[80] Noman AS, Koide N, Hassan F, I IE-K, Dagvadorj J, Tumurkhuu G, Islam S, Naiki Y, Yoshida T, Yokochi T (2009) Thalidomide inhibits lipopolysaccharide-induced tumor necrosis factor-alpha production via down-regulation of MyD88 expression. *Innate Immun* **15**, 33-41.

[81] Eljaschewitsch E, Witting A, Mawrin C, Lee T, Schmidt PM, Wolf S, Hoertnagl H, Raine CS, Schneider-Stock R, Nitsch R, Ullrich O (2006) The endocannabinoid anandamide protects neurons during CNS inflammation by induction of MKP-1 in microglial cells. *Neuron* **49**, 67-79.

[82] Ramirez BG, Blazquez C, Gomez del Pulgar T, Guzman M, de Ceballos ML (2005) Prevention of Alzheimer's disease pathology by cannabinoids: neuroprotection mediated by blockade of microglial activation. *J Neurosci* **25**, 1904-1913.

[83] Pineda FJ (1987) Generalization of back-propagation to recurrent neural networks. *Physical Review Letters* **59**, 2229-2232.

[84] Pineda FJ (1989) Recurrent backpropagation and the dynamical approach to adaptive nerual computation. *Neural computation* **1**, 161-172.

[85] Anastasio TJ (2009) *Tutorial on neural systems modeling*, Sinauer Associates, Incorporated.

[86] Thomas R, d'Ari R (1990) *Biological feedback*, CRC press.
[87] Rumelhart DE, McClelland JL, Group PR (1987) *Parallel distributed processing*, MIT press Cambridge, MA.
[88] LeCun Y, Bengio Y (1995) Convolutional networks for images, speech, and time series. *The handbook of brain theory and neural networks* **3361**, 1995.
[89] LeCun Y, Bengio Y, Hinton G (2015) Deep learning. *Nature* **521**, 436-444.
[90] Payan A, Montana G (2015) Predicting Alzheimer's disease: a neuroimaging study with 3D convolutional neural networks. *arXiv preprint arXiv:1502.02506*.